

NASA Contractor Report 178013

NASA-CR-178013
19860004028

**ELASTIC-PLASTIC DEFORMATION OF A
METAL-MATRIX COMPOSITE COUPON
WITH A CENTER SLOT**

**Daniel Post, Robert Czarnek,
Duksung Joh, Jinmyun Jo, and Yifan Guo**

**VIRGINIA POLYTECHNIC INSTITUTE
AND STATE UNIVERSITY
Blacksburg, Virginia**

**Grant NAG1-343
November 1985**

NASA
National Aeronautics and
Space Administration
Langley Research Center
Hampton, Virginia 23665

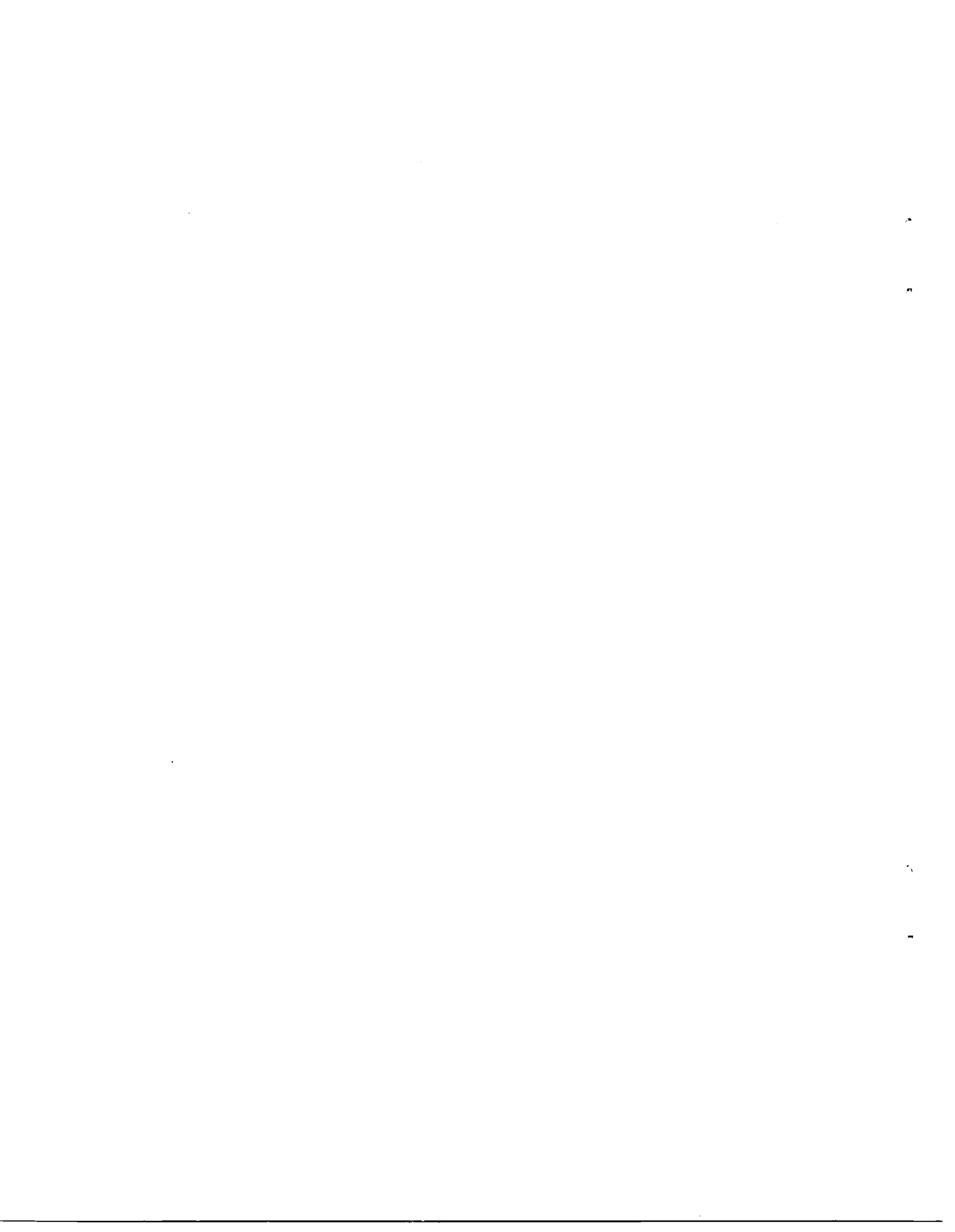
FOR REFERENCE

NOT TO BE TAKEN FROM THIS ROOM

LIBRARY COPY

DEC 12 1995

LANGLEY RESEARCH CENTER
LIBRARY, NASA
HAMPTON, VIRGINIA



9 1 1 RN/NASA-CR-178013

86N13496**# 1.26:178013
DISPLAY 09/6/1
ISSUE 4 PAGE 584 CATEGORY 27 RPT#: NASA-CR-178013 NAS
CNT#: NAG1-343 85/11/00 49 PAGES UNCLASSIFIED DOCUMENT

UTTL: Elastic-Plastic deformation of a metal-matrix composite coupon with a center slot

AUTH: A/POST, D.; B/CZARNEK, R.; C/JOH, D.; D/JO, J.; E/GUO, Y.
CORP: Virginia Polytechnic Inst. and State Univ., Blacksburg. CSS: (Dept. of Engineering Science and Mechanics.) AVAIL.NTI5

SAP: RC A03/MF A01

CIO: UNITED STATES

MAJS: /*ALUMINUM/*BORON FIBERS/*DEFORMATION/*DISPLACEMENT MEASUREMENT/* ELASTOPLASTICITY/*INTERFEROMETRY/*METAL MATRIX COMPOSITES/*MOIRE EFFECTS/*

MINS: PLASTIC DEFORMATION/*SAMPLES/*SHEAR STRAIN/*SLOTS/*STRESS CONCENTRATION / EVALUATION/ EXPERIMENTATION/ LOADS (FORCES)/ MECHANICAL PROPERTIES

ABA: Author

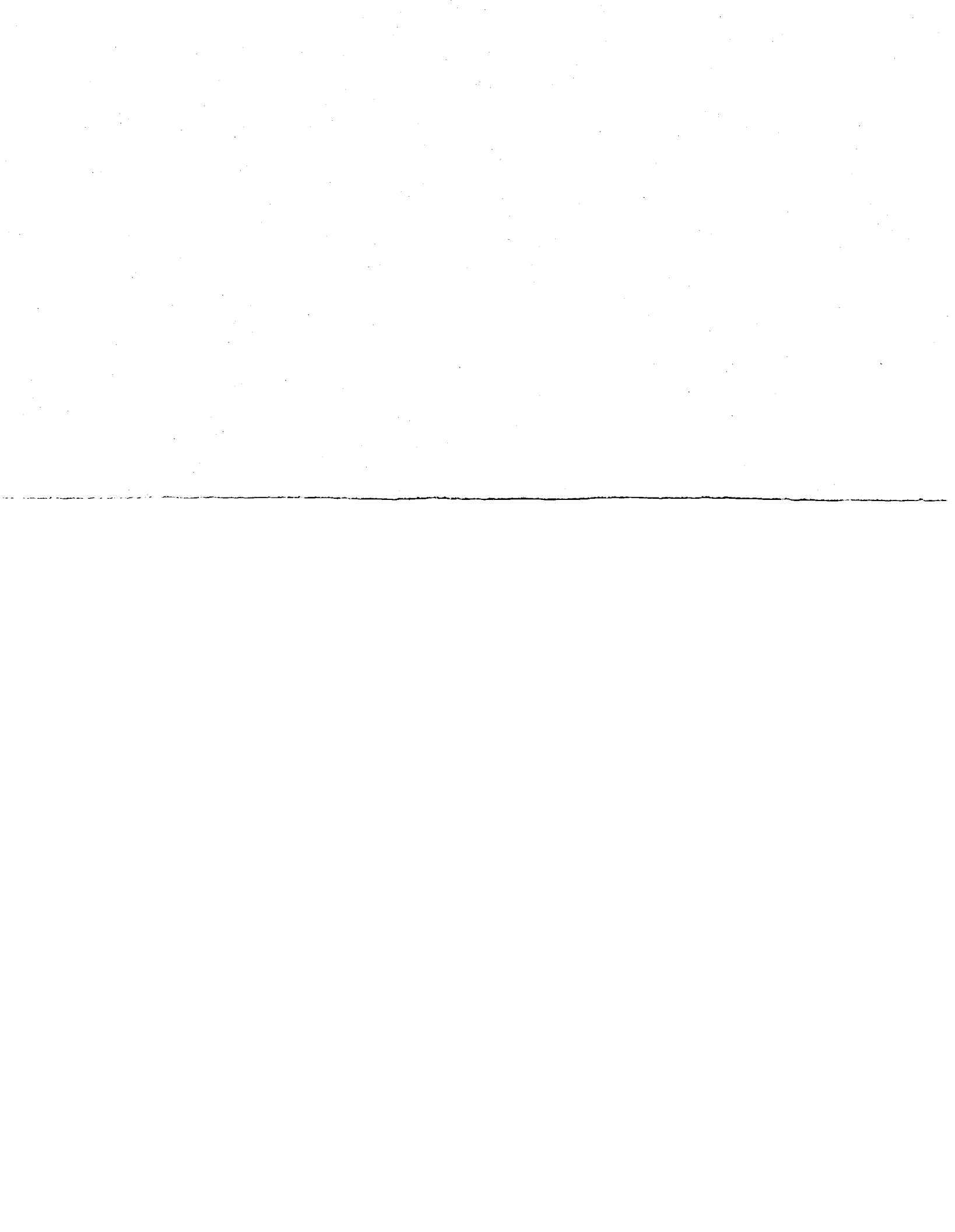


TABLE OF CONTENTS

	<u>Page</u>
ABSTRACT	1
INTRODUCTION	2
EXPERIMENTAL METHOD: MOIRE INTERFEROMETRY	3
TEST PROCEDURE, MOIRE PATTERNS	4
ANALYSIS, QUALITATIVE	5
ANALYSIS, QUANTITATIVE	7
CONCLUSIONS	12
ACKNOWLEDGEMENTS	13
REFERENCE	13
TABLE I	14
FIGURES	15



ABSTRACT

A comprehensive experimental analysis of deformations of the surface of a metal-matrix specimen is reported. The specimen was a 6-ply $[0/\pm 45]_S$ boron-aluminum tensile coupon with a central slot. Moire interferometry was used for high-sensitivity whole-field measurements of in-plane displacements. Normal and shear strains were calculated from displacement gradients. Displacement fields were analyzed at various load levels from 15% to 95% of the failure load. Deformations of the boron fibers could be distinguished from those of the matrix.

Highly localized plastic slip zones occurred tangent to the ends of the slot. Shear strains and concurrent transverse compressive strains in the slip zones reached approximately 10% and 1%, respectively. Upon unloading, elastic recovery in surrounding regions caused a reverse plastic shear strain in the slip zone of about 4%.

Longitudinal normal strains on the unslotted ligament peaked at the slot boundary at about 1% strain. The strain concentration factor at the end of the slot decreased with load level and the advance of plasticity.

KEY WORDS

composites
metal-matrix
elastic-plastic
deformation fields
strain distributions
plastic slip
moire interferometry
experimental analysis

INTRODUCTION

Understanding, and rational design, with metal-matrix composites requires phenomenological evidence obtained from detailed measurements of its behavior. Experimental analysis of a tensile coupon with a severe stress concentration, a central slot, was undertaken here. The objective was a detailed determination of deformations in the vicinity of the slot, including the redistribution of deformations at higher loads -- where the ductile matrix exhibited plastic deformations. Quantitative observations were made up to 95% of the failure load. The composite was boron/aluminum, with a 6-ply stacking sequence $[0/\pm 45]_S$. Its composition is given in Fig. 1, together with the specimen geometry.

Deformations were determined by moire interferometry. This is an optical method that produces whole-field contour maps of in-plane displacement components u_x and u_y . Sensitivity is in the subwavelength range, namely 16.4×10^{-6} inches per fringe order. In addition to high sensitivity, it is characterized by high contrast interference fringes and high spatial resolution, permitting detailed analysis of both global and localized deformations. Normal strains and shear strains can be determined from the displacement information. While it is similar in many ways to classical and holographic interferometry -- which are techniques primarily useful for out-of-plane displacement measurements, u_z -- moire interferometry provides the important in-plane displacements, u_x and u_y .

EXPERIMENTAL METHOD: MOIRE INTERFEROMETRY

A comprehensive description of moire interferometry appears in Ref. 1. Briefly, a high frequency crossed-line diffraction grating is replicated on the specimen surface using a special mold, as illustrated in Fig. 2a. The result is a thin -- usually 0.001 in. -- reflective phase grating firmly adhered to the specimen, which deforms together with the specimen surface. The specimen grating is observed in an optical arrangement illustrated schematically in Fig. 2b. Two beams of light incident at angles α and $-\alpha$ form a virtual reference grating, with its grating lines perpendicular to the plane of the figure. Its frequency is $f = (2 \sin \alpha)/\lambda$, where λ is the wavelength of the light. This reference grating interacts with the similarly oriented lines of the specimen grating to form the interference pattern recorded in the camera. When the reference grating lines are perpendicular to the x axis, the pattern is a contour map of displacements governed by the relationship

$$u_x = \frac{1}{f} N_x \quad (1)$$

where u_x is the in-plane x component of displacement at any point and N_x is the fringe order at that point in the fringe pattern.

The crossed-line specimen grating was applied in the xy plane with lines perpendicular to the x and y axes. In the optical arrangement used in these experiments, two additional beams (not shown) produced a virtual reference grating perpendicular to that of Fig. 2b. Individual patterns of N_x or N_y were obtained by blocking the light of the alternate virtual reference grating. When the reference grating lines were perpendicular to the y axis, in-plane displacements u_y were obtained from fringe orders N_y by

$$u_y = \frac{1}{f} N_y \quad (2)$$

Frequency f was 60,960 lines/in. (2400 μ /mm). An argon ion laser was used at wavelength 20.3 μ in. (0.514 μ m) and 100 mW power.

Strains can be calculated from the displacement fields by the (small strain) relations

$$\epsilon_x = \frac{\partial u_x}{\partial x} = \frac{1}{f} \frac{\partial N_x}{\partial x} \quad (3)$$

$$\epsilon_y = \frac{\partial u_y}{\partial y} = \frac{1}{f} \frac{\partial N_y}{\partial y} \quad (4)$$

$$\gamma_{xy} = \frac{\partial u_x}{\partial y} + \frac{\partial u_y}{\partial x} = \frac{1}{f} \left(\frac{\partial N_x}{\partial y} + \frac{\partial N_y}{\partial x} \right) \quad (5)$$

The accuracy of the calculated strains is substantially less than the accuracy of the displacements. Regardless of the method used to determine the derivatives, differentiation of experimental data always results in a band of uncertainty that is much broader than the uncertainty in the data. However, satisfactory strain determinations are achieved in the present work because the closely spaced fringes of the displacement fields provide an abundance of high accuracy data.

TEST PROCEDURE, MOIRE PATTERNS

The metal-matrix specimen was supplied by NASA Langley Research Center; the central slot was produced by an electric spark discharge technique. The specimen grating and electric resistance strain gage (1/4 inch gage length, gage CEA-06-250 UW-350, Measurements Group Inc., Raleigh, NC) indicated in Fig. 1 were applied at VPI & SU. The specimen was installed in a mechanical loading fixture equipped with strain gage transducers to measure the applied load, P ; the fixture was attached to

a vibration isolation table that also supported the optical elements of the moire interferometry system.

Following initial adjustments, the specimen was loaded in a sequence of loading steps; for each step the load and strain gage readings were recorded and the N_x and N_y patterns were photographed. After loading to 95% of the predicted failure load, the load was removed and patterns of the residual displacement fields were photographed. Relevant loading data are shown in Table I. The predicted failure load, P_f , is the average of failure loads for similar specimens tested at NASA Langley Research Center.

The moire interferometry fringe patterns of N_y and N_x are shown in Figs. 3(a) - 3(l) for loads P/P_f ranging between 15% and 95%. The residual displacement fields, after the specimen was unloaded to 1.3% of P_f , are shown in Figs. 4(a),(b).

ANALYSIS, QUALITATIVE

At 15% of P_f (Fig. 3a), the fringes are most closely spaced near the ends of the slot, indicating zones of largest displacement gradients or strains. The fringes are smoothly or systematically spaced, however, in contrast to the abrupt changes in fringe gradients seen in the N_y patterns for all the higher loads. These abrupt changes, which occur in narrow vertical zones tangent to the slot ends, are strong concentrations of shear strains; they are undoubtedly associated with localized plasticity of the matrix material which permits relative slip of the 0° boron fibers in the outer ply. They will be called plastic slip zones. Whereas the intensity of these shear strains and fiber displacements increases with load level, it is curious that the length

of each slip zone increases rather slowly, much more slowly than proportional to the load.

On the left side, the slot seems to terminate partly through a boron fiber. That fiber appears to have broken at a load between 15% and 25% of the failure load. The apparent break first appears in Fig. 3(c), along the centerline of the slot. On the right side, the slot appears to terminate in the matrix material and the first continuous fiber beyond the slot remains unbroken throughout the test.

The N_x patterns show that compressive strains are substantially larger in the slip zone than in surrounding regions. Plasticity in the matrix comprising the slip zone appears to be accompanied by two conditions, elevated compressive strains and large shear strains.

The first evidence of inter-fiber plasticity occurs between the first continuous fiber outside the slot and the neighboring fiber intercepted and cut by the slot. Subsequently, at a higher load, severe plastic deformation appears to develop in the matrix between the next inboard pair of fibers (toward the specimen centerline), where a second slip zone is formed.

Except for the lowest load levels, N_y fringes near the slip zones are seen to have an irregular or zig-zag character. These are real deformation effects, and not optical noise in the experiments. They signify larger values of $\partial u_y / \partial x$ in the matrix and smaller values in the fibers. This translates to larger shear strains in the matrix between fibers and smaller shear strains in the fibers.

The N_x fringes show a similar cyclical behavior above and below the center of the slot. This is where the average compressive ϵ_x strains are large. The zig-zag fringes in this region are especially pronounced

in Figs. 3(j) and 3(1). They have relatively horizontal segments, where $\partial u_x / \partial X$ is very small, and inclined segments where $\partial u_x / \partial X$ is large. The former corresponds to fiber locations (where ϵ_x is small) and the latter to matrix locations (where ϵ_x is large). The period of the cyclic disturbances is 0.007 in., which corresponds to the fiber spacing. In both cases -- shear along the fibers and compression across the fibers -- the deformation proceeds in harmony with the compliance of the material and deformations are larger in the more compliant matrix.

In fact, the magnitude of this disparity of deformations in matrix and fibers is somewhat masked by the experimental method. While the specimen grating is very thin, its thickness is finite. Shear lag in the grating thickness introduces some difference between the deformations at the surface of the specimen and at the surface of the grating. The effect appears to be small enough that it will not change the trends or influence the conclusions of these tests.

Figure 4 shows dramatic residual deformations. Permanent deformations are evident throughout the field, even far from the slot. Strong permanent deformations are evident in the slip zones tangent to the slot ends and in the compression zones near the center of the slot.

ANALYSIS, QUANTITATIVE

Figure 5 shows the stress-strain curve for the specimen at zones remote from the slot. The data correspond to those in Table I, where the far-field strains are determined by the strain gage. The longitudinal stress-strain behavior is mildly non-linear from low stress levels to 95% of the specimen failure load.

Figures 6 and 7 are plots of the u_y and u_x displacements near the slot. Figure 6 shows the displacements for one load level, $P/P_f = 80\%$, for the 4 horizontal lines indicated in the figure. The displacements for 4 load levels are plotted in each of Figs. 7(a)-(d), but for different distances from the slot. The figures show the gradual intensification of displacement gradients at locations approaching the slot; and they show the gradual intensification of gradients with increase of load.

These data, and those used in all subsequent figures, were taken from the first quadrant (upper-right section) of the fringe pattern. While deformations in the four quadrants are not identical, they are sufficiently similar that the results for the first quadrant can be taken to represent the behavior of the entire specimen.

In Figs. 6 and 7, the line segments of very large slopes, at and near $x = 0$, correspond to the slip zones. These segments are drawn as straight lines, since fringes in these very narrow zones were not resolved. The shear strains interpreted from these straight segments are assumed to be uniform across the width of the slip zone. It is possible and even probable that these displacements would be better represented by shallow S-shaped curves, which would lead to higher values of shear strains along the centerline of the slip zone. Accordingly, shear strains in the slip zone are assessed conservatively in the subsequent figures.

Figure 8 shows the distributions of strains along the y and x axes for one load level, $P/P_f = 80\%$. In (a) the normal and shear strains are plotted as a function of distance along the y axis; in (b) the normal strains are plotted against distance along the x axis. Note the

different scales for ϵ_x and ϵ_y , indicating they have opposite signs. Clearly, the shear strains near the slot are very much larger than the normal strains. This high shear strain is the dominant feature in the specimen deformation. The peak shear reaches a strain level near 8%, well into the plastic range of the matrix material. The peak shear occurs near the slot, but it is located above the centerline of the slot; at the centerline, the shear strain must be zero.

Figure 8(b) illustrates the normal strains along the unslotted ligament. The peak value of ϵ_y occurs at the slot boundary, but it is an order of magnitude smaller than the peak shear strain.

Normal strain ϵ_x is very small at the slot boundary, indicating a very small effective Poisson's ratio at that point. This may be associated with the underlying $\pm 45^\circ$ fibers; these fibers are not continuous, but instead they terminate at the slot boundary. Remote from the slot, at $x = 1.3a$ and $y = 0$, the ratio ϵ_x/ϵ_y is approximately 0.2.

A comparison is made in Fig. 9 of the shear strains along the y axis (along the line marked A) and along the adjacent line marked B. The load level was $P/P_f = 80\%$. The severe plastic deformation along line B began at a higher load level and the peak shear strain along B remained substantially lower than that along A -- where severe plastic deformation first appeared.

Figure 10 shows the residual strains along the y and x axes, after the load was reduced to only 1.3% of P_f . The residual shear strains (Fig. 10a) are large, peaking at about 4.7% strain. For comparison, the peak shear strain at the highest load level ($P/P_f = 95\%$) was about 8.8% strain. The difference (4.1% shear strain) cannot be attributed to

elastic recovery since a recovery of several percent cannot be elastic. Instead, the elastic recovery of adjacent regions of the specimen, including the underlying $\pm 45^\circ$ plies, must have caused a reverse plastic deformation in the high shear zones. This suggests that low-cycle fatigue might be an important parameter in the material performance.

Comparing the normal strains in the slip zone (Figs. 10a and 8a), residual longitudinal strains ϵ_y are relatively low near the slot. This signifies substantial recovery from the maximum load condition. On the other hand, residual transverse strains ϵ_x are more than half as large as those for the maximum load condition, indicating a modest recovery. While these compressive strains in the maximum load conditions were only 0.1% and less, the matrix material in that zone was well into its plastic state because of the very high shear strains; the absence of strong recovery of these small compressive strains is attributed to the plasticity of the matrix.

The longitudinal residual strains, ϵ_y , along the x axis (Fig. 10b) are nearly constant remote from the slot. Near the slot, however, they dip to a low residual strain level. The change of shape of the curve, relative to the ϵ_y curve for the loaded condition (Fig. 8b), is curious. What might be viewed as excessive recovery of ϵ_y near the slot must result from a different mode of deformation in the unloading process, relative to that in the loading process. An explanation such as work-hardening of the matrix would fit the observation, wherein more plastic deformation would occur during loading than unloading.

Figures 11(a) and 11(b) show plots of longitudinal strains ϵ_y along the x axis for various load levels; in (a) the strains are normalized with respect to the far-field strain ϵ_{ff} , while in (b) they are

normalized with respect to the far-field stress, σ . Normalization with respect to far-field strain seems the more informative.

Remote from the slot, the curves cluster together (Fig. 11a), indicating that strains in the remote regions are essentially proportional to the load. More accurately, these normalized strains rise gradually with load level -- consistent with Fig. 5, which shows a gradual increase of compliance with stress level.

Very close to the slot, the behavior is reversed (Fig. 11a). Normalized strains ϵ_y/ϵ_{ff} decrease as the applied load increases. Strains ϵ_y are rather high in this region, and the matrix material becomes increasingly plastic as the load increases. This presumably distributes the local forces more effectively to adjacent fibers and depresses the strain concentration that would otherwise be developed.

Figure 12 shows the strain concentration ϵ_y/ϵ_{ff} at the end of the slot as a function of applied load on the specimen. This strain concentration reduces significantly with load level, from about 8 at 15% of failure load to about 4 at 95% of failure load. The trend of the curve is clear, although scatter of data points is greater here than in preceding graphs. This is because the moire fringes surrounding these points of peak strain are less distinct than elsewhere.

Figures 13(a) and (b) show the shear strains along the y axis, where they are normalized with respect to far-field strains and stresses, respectively. The character of the curves for different load levels is basically the same, except for the 15% load, which shows a much smaller shear strain concentration near the slot. At higher loads, the plastic slip band (in the matrix adjacent to the first continuous fiber) is fully developed and the curves represent shear strains in this slip zone.

Shear strains in the slip zone are, by far, the highest strains developed in the specimen, higher than others by an order of magnitude. Their magnitudes are undoubtedly underestimated, too, for reasons already mentioned -- shear lag through the grating thickness and averaging across the slip zone. The region of highest shear strain occurs in a very small part of the slip zone, but very substantial shear strains occur throughout the slip zone.

Figure 14 is a plot of the shear concentration $\gamma_{xy}/\epsilon_{ff}$, at the point where γ_{xy} is maximum, as a function of load level. This strain concentration becomes exceedingly high as soon as the slip zone is formed, and it continues to rise with the load. The dashed line represents an estimate of performance at lower load levels, where the strain concentration is assumed to be nearly constant prior to development of the slip zone.

CONCLUSIONS

A comprehensive experimental analysis of deformations of the surface of a metal-matrix tensile specimen with a central slot is reported. Deformations, specifically in-plane displacements and strains, were determined at several load levels, from 15% to 95% of the failure load. Deformations of the fibers could be discriminated from those of the matrix.

The dominant feature of deformation was a plastic slip zone tangent to the end of the slot. It occurred in the matrix material adjoining the last continuous fiber adjacent to the slot. At 95% of the failure load, shear strains in the slip zone reached approximately 10%. Concurrently, compressive normal strains acting perpendicular to the

slip zone reached approximately 1%. The matrix material exhibited highly plastic behavior. The shear strain concentration factor $\gamma_{xy}/\epsilon_{ff}$, where ϵ_{ff} is the far-field longitudinal strain, jumped to a value of 23 when the slip band first occurred, and it rose to about 30 at 95% of the failure load.

Longitudinal normal strains on the unslotted ligament (x axis) peaked at the slot boundary at about 1% strain, which was well into the plastic range of the matrix material. This strain concentration factor decreased with the advance of plasticity from about 8 to about 4.

Upon unloading from 95% of the failure load, permanent deformation remained throughout the specimen. Residual shear strain and residual compressive strain in the slip zone reached approximately 5% and 0.6%, respectively. Elastic recovery in surrounding regions caused a reverse plastic shear strain in the slip zone of about 4%. Along the unslotted ligament, the residual longitudinal strain peaked at a significant distance from the slot at about 0.1% strain.

ACKNOWLEDGEMENTS

Dr. W. S. Johnson of NASA Langley Research Center was the NASA Technical Office for this research. His assistance and valuable discussions are greatly appreciated.

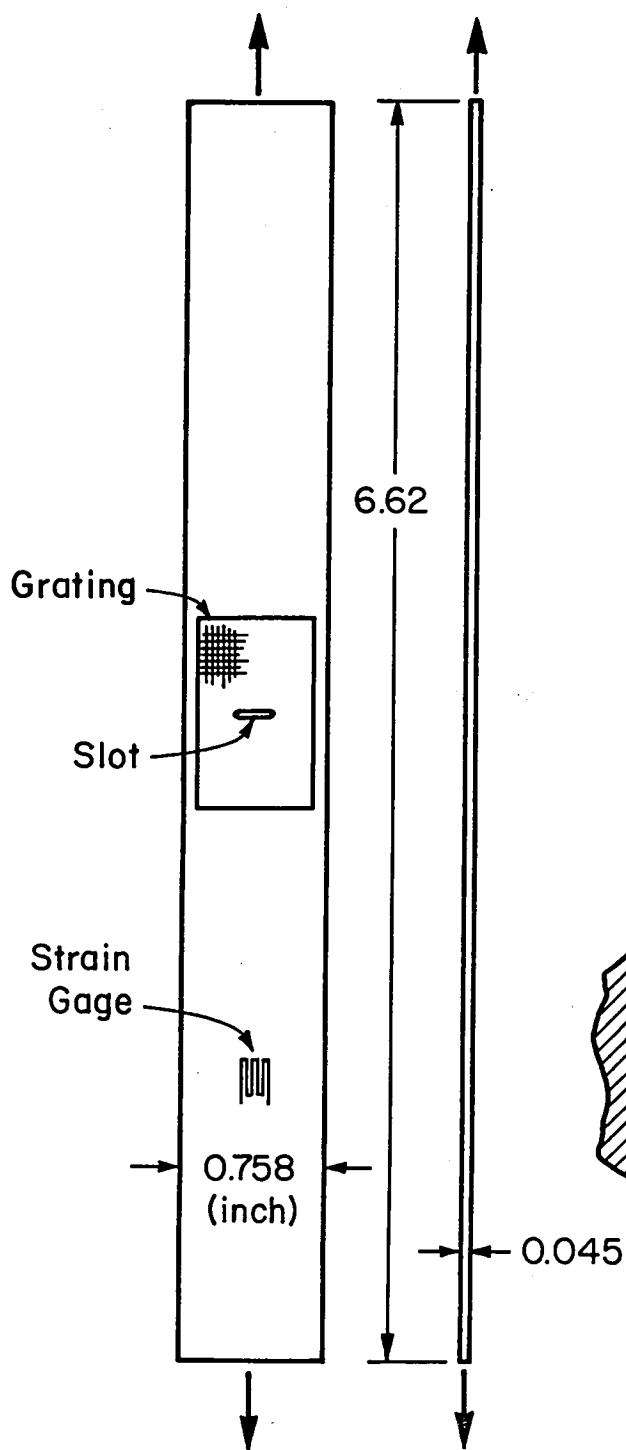
REFERENCE

1. Post, D., "Moire Interferometry at VPI & SU," Experimental Mechanics, 23(2), June 1983, pp. 203-211.

TABLE I
LOAD AND FAR-FIELD STRESS AND STRAIN

Load, P (lbs)	% Failure load* (P/P _f)	Far-field	
		Strain, ϵ (μ in./in.)	Stress, σ (psi)
200	15%	290	5,860
336	25%	555	9,850
538	40%	1025	15,800
803	60%	1700	23,500
1070	80%	2410	31,400
1270	95%	3010	37,200
18	1.3%	710	530

*P_f = Failure load (average) = 1340 lbs.



Specimen

Metal Matrix Composite

6 ply layup $[0/\pm 45]_s$

Boron/Aluminum

boron fiber dia. = 0.14 mm

44% fiber by volume

Aluminum 6061 annealed

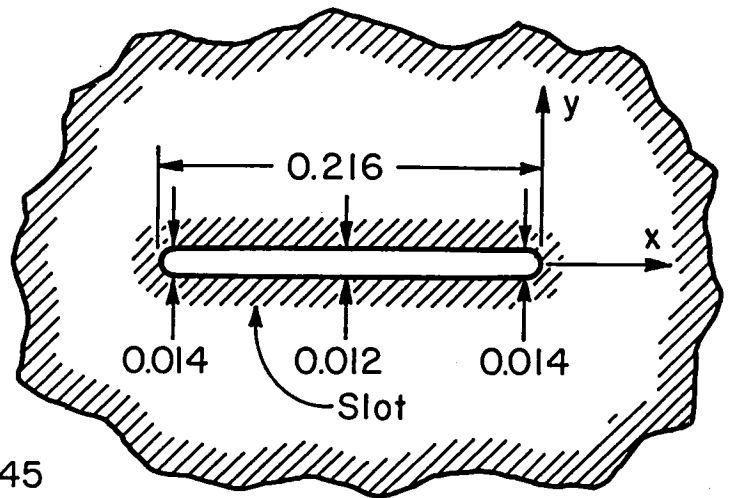


Fig. 1 Specimen and loading.

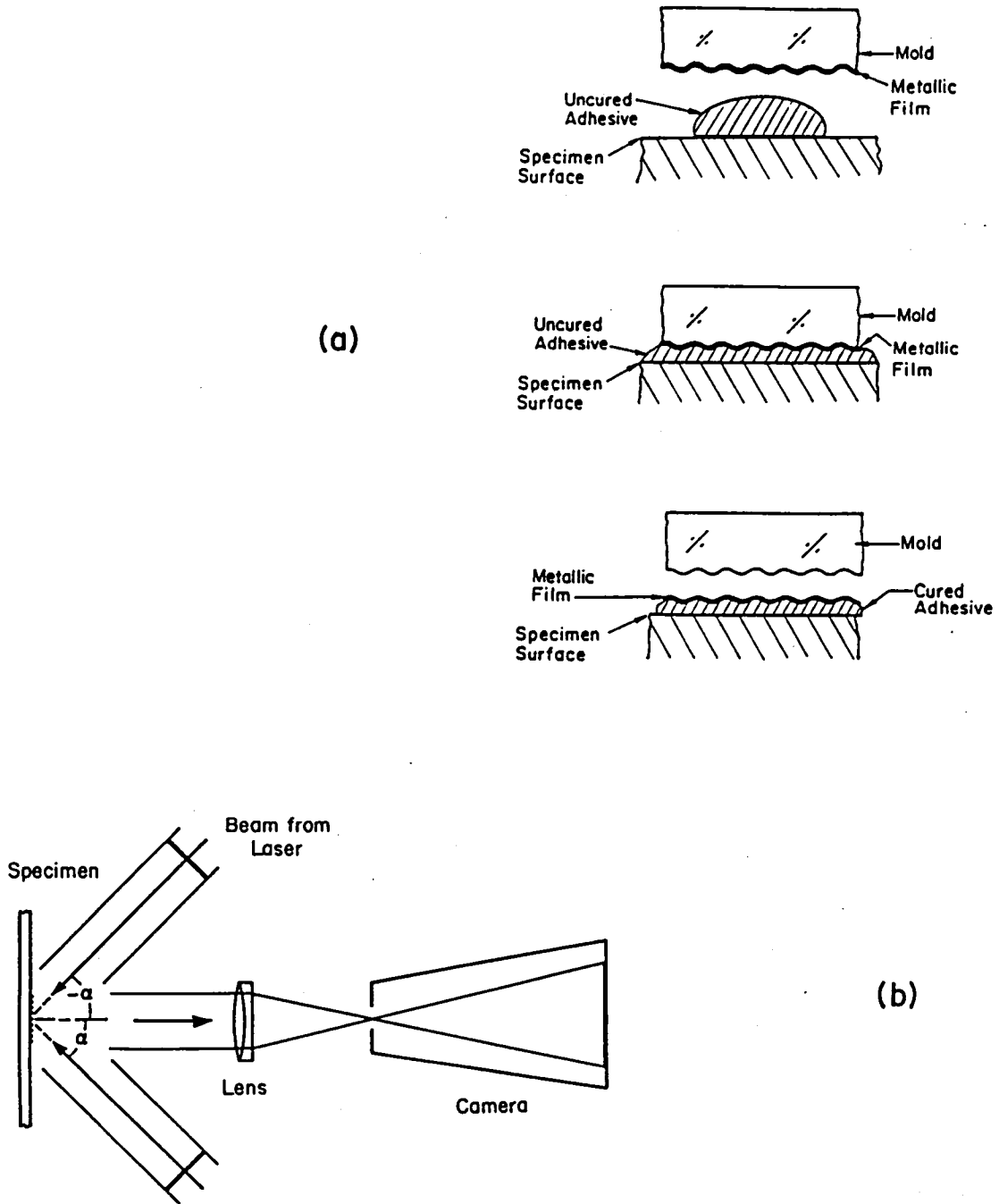


Fig. 2 (a). Replication technique to form a high-frequency, high-reflectance grating on the specimen.
 (b). Optical arrangement for moire interferometry.

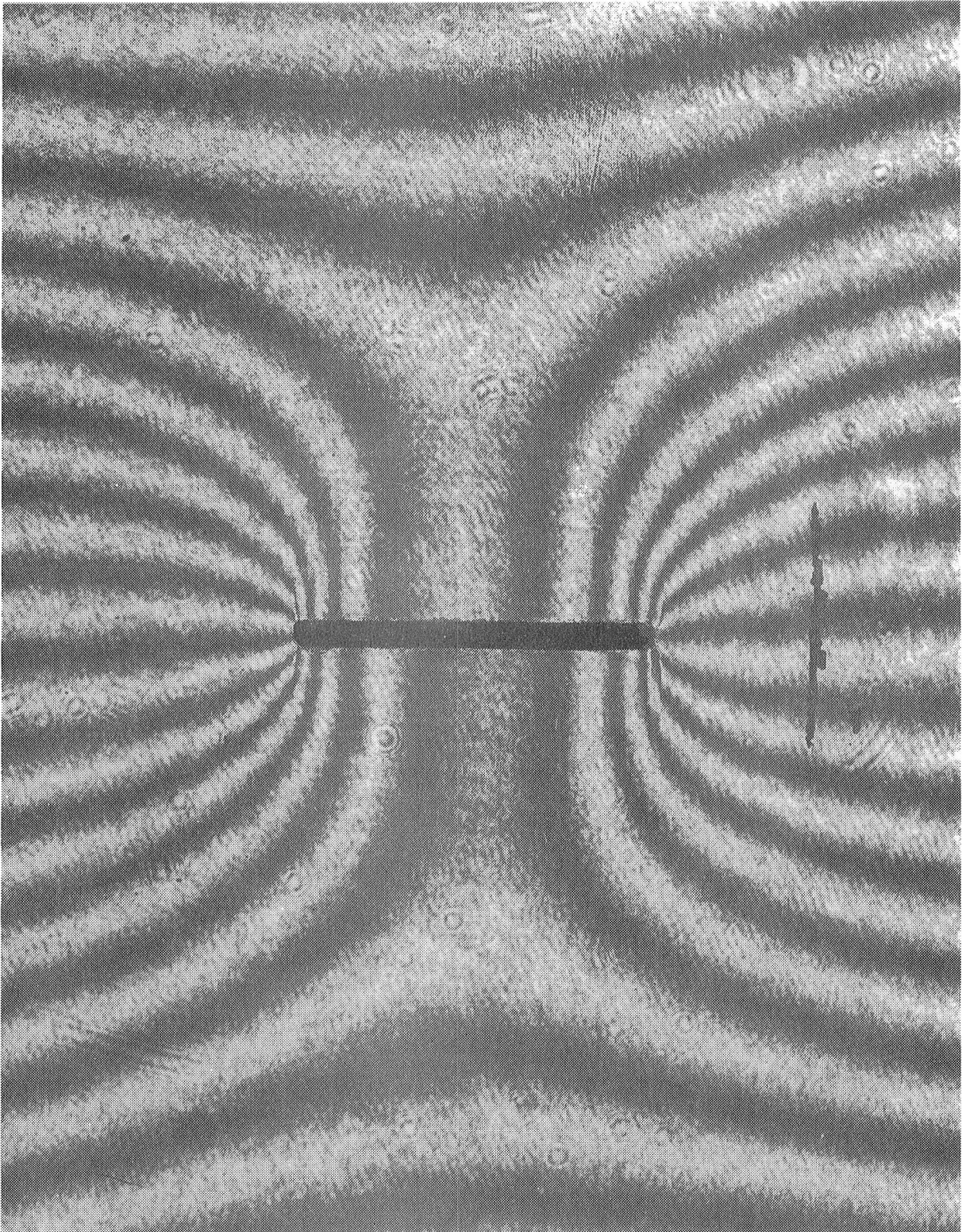


Fig. 3 (a). N_y pattern depicting the u_y displacement field. Contour interval is $16.4 \mu\text{in./fringe order}$ in all patterns. $P/P_f = 15\%$.

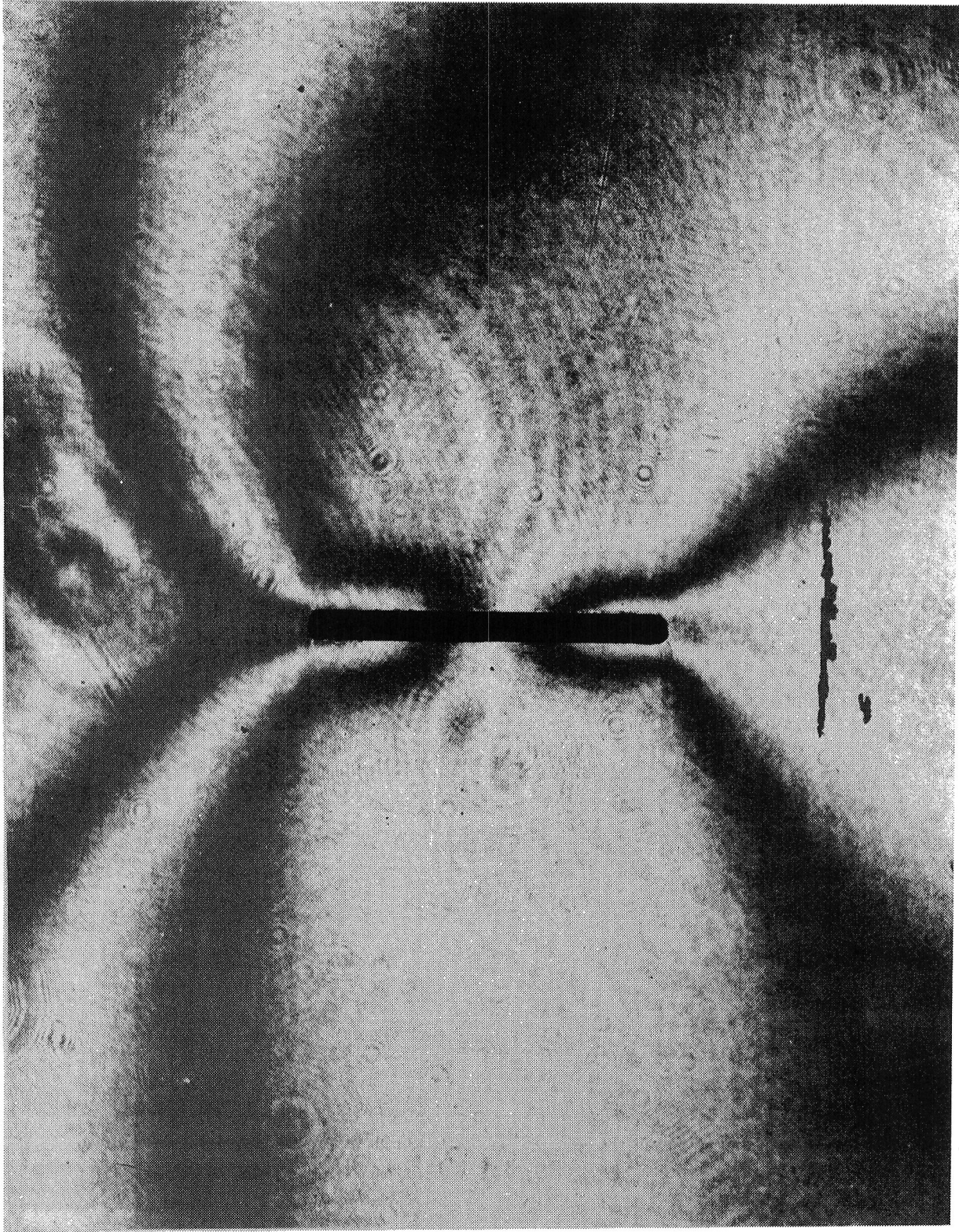


Fig. 3 (b). N_x pattern for $P/P_f = 15\%$.

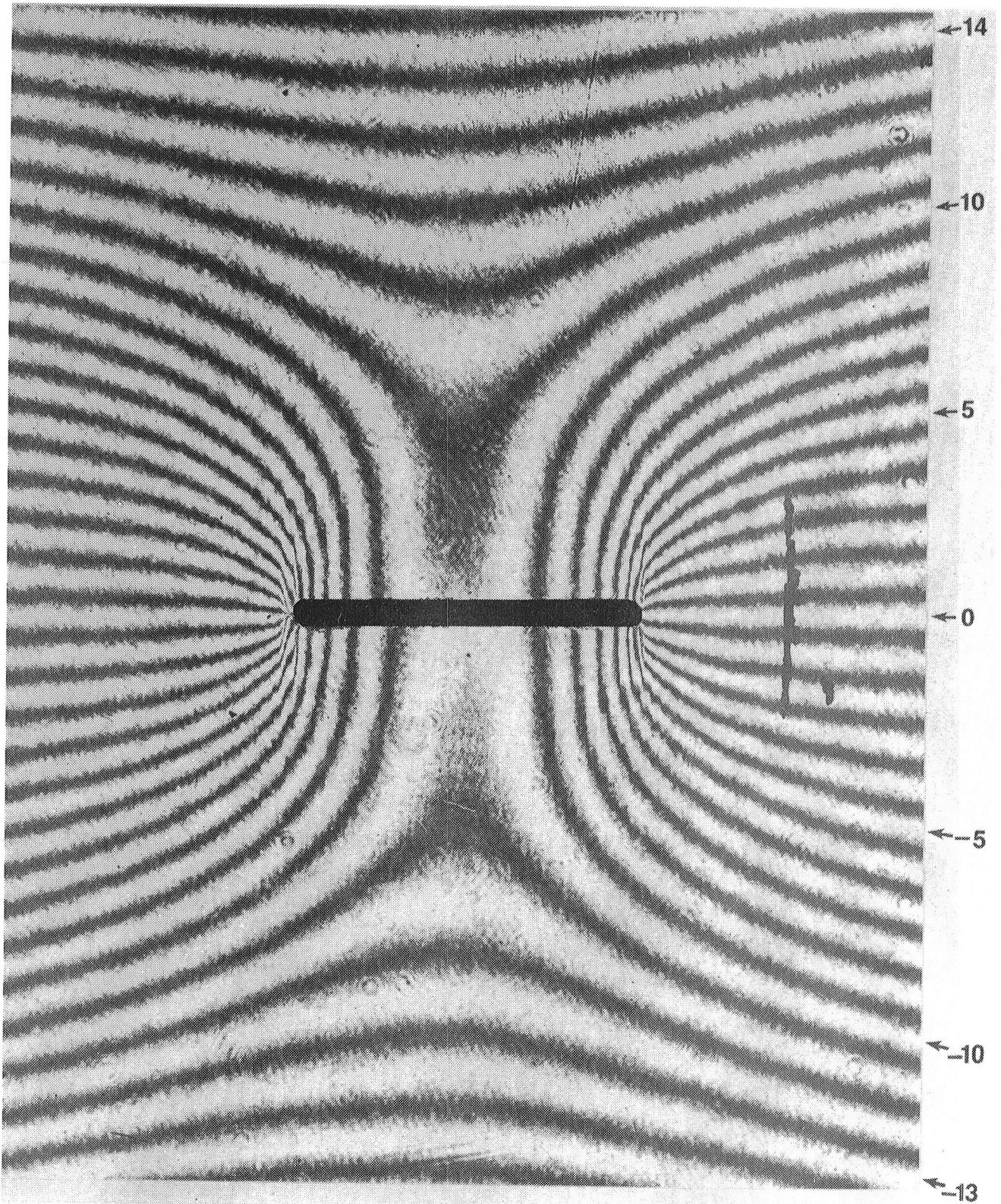


Fig. 3 (c). N_y pattern for $P/P_f = 25\%$. Numbers give the numerical values of fringe orders N_y for each contour line, i.e., along the centerline of each fringe.

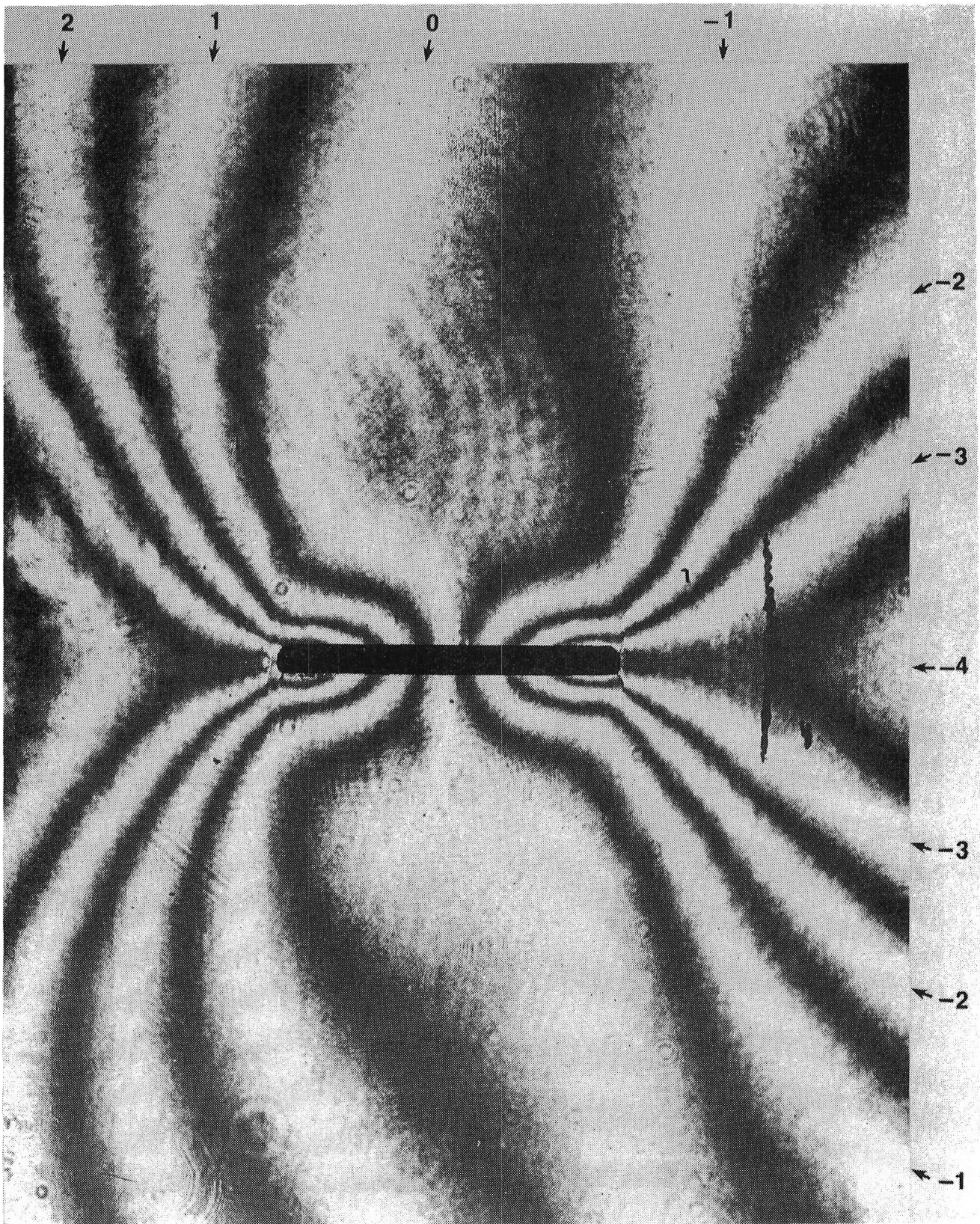


Fig. 3 (d). N_x pattern for $P/P_f = 25\%$. Numbers give the numerical values of N_x .

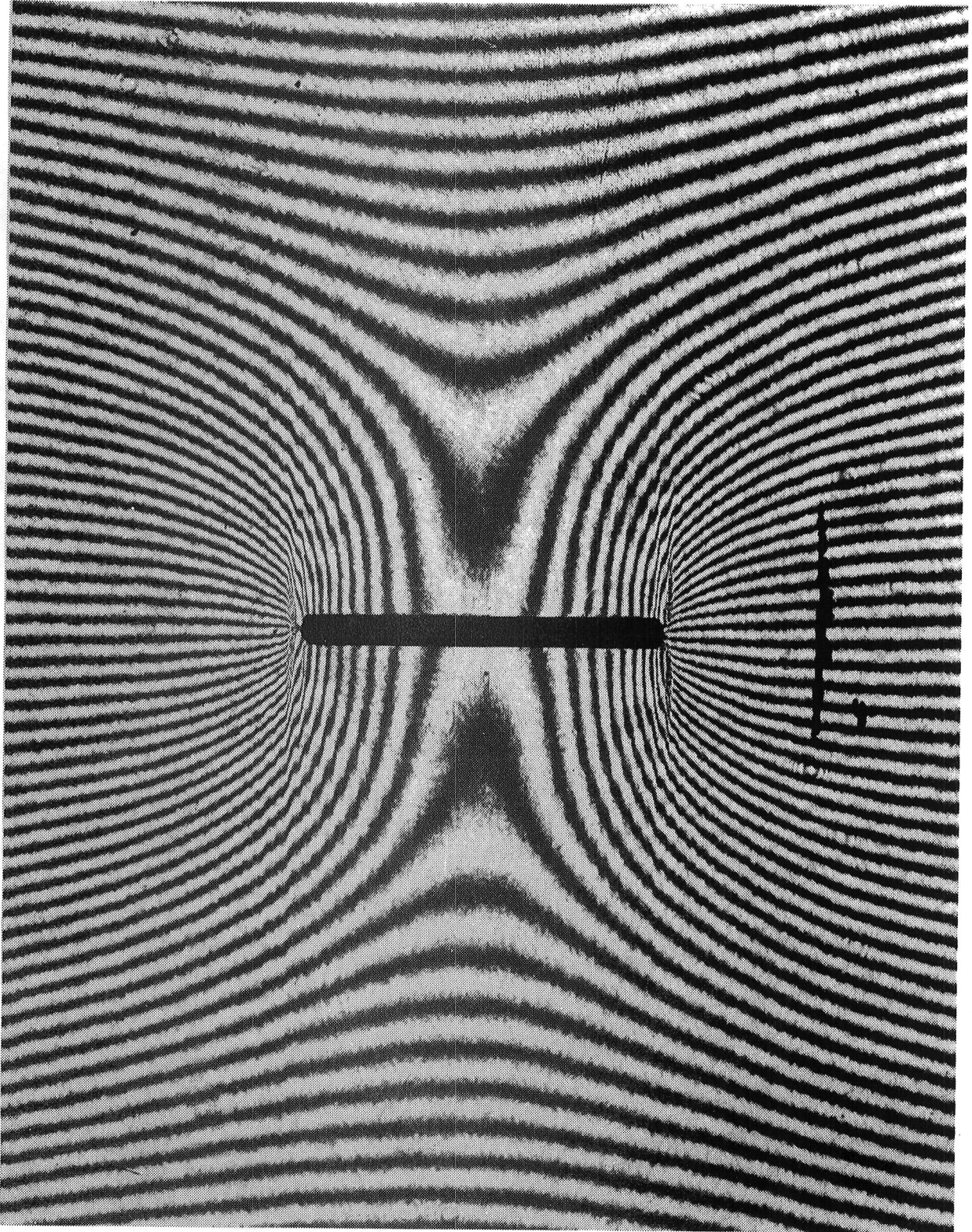


Fig. 3 (e). N_y pattern for $P/P_f = 40\%$.

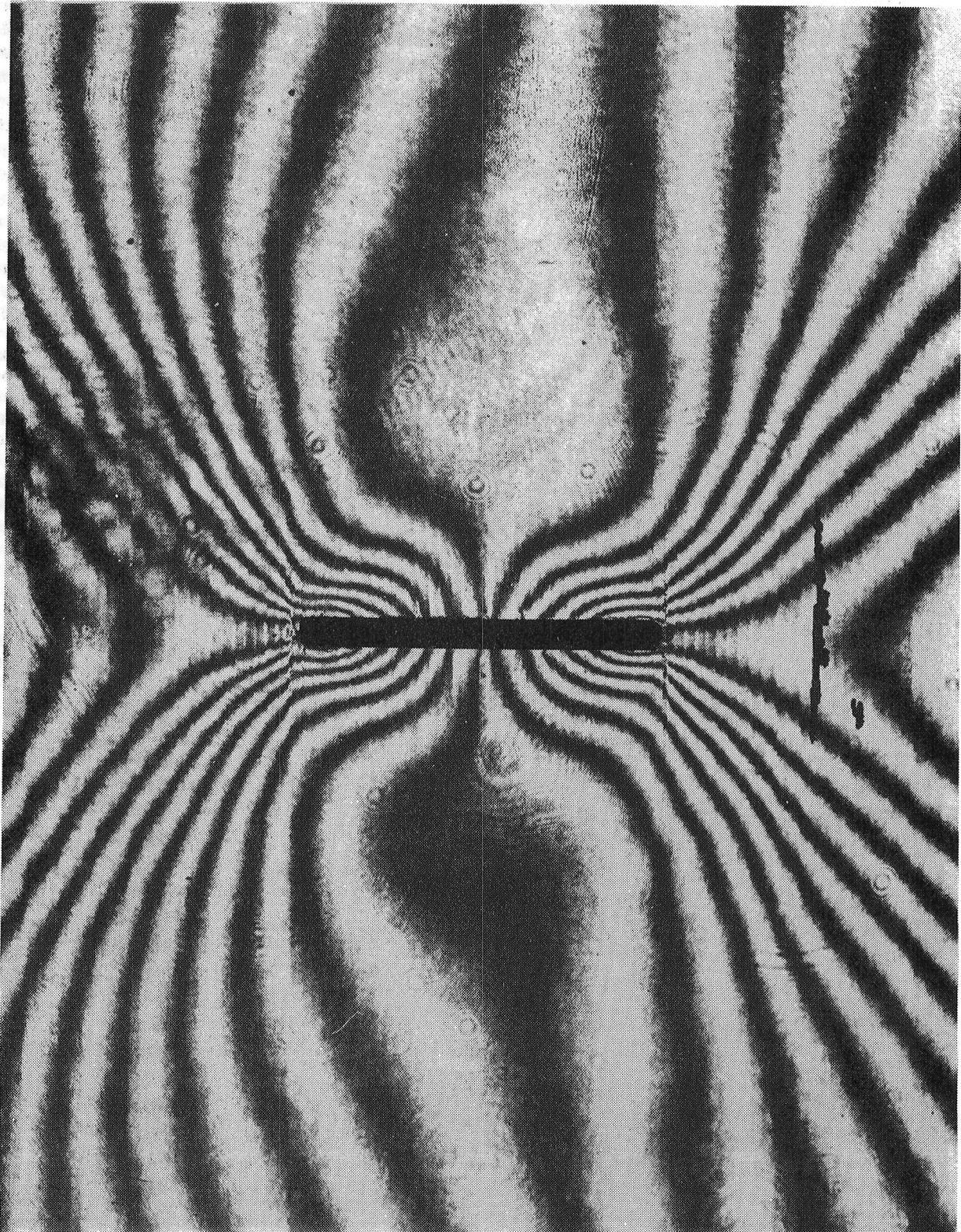


Fig. 3 (f). N_x pattern for $P/P_f = 40\%$.

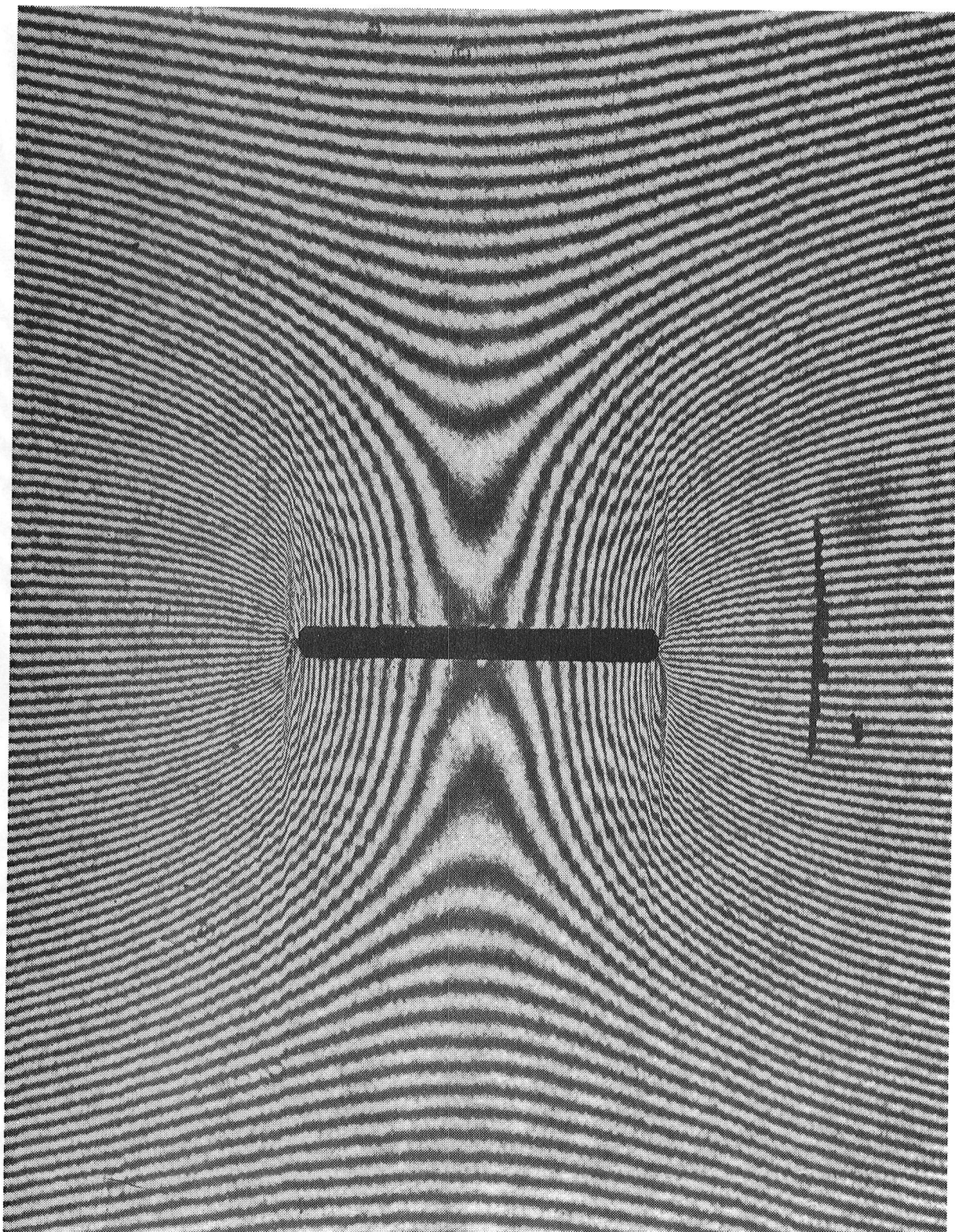


Fig. 3 (g). N_y pattern for $P/P_f = 60\%$.

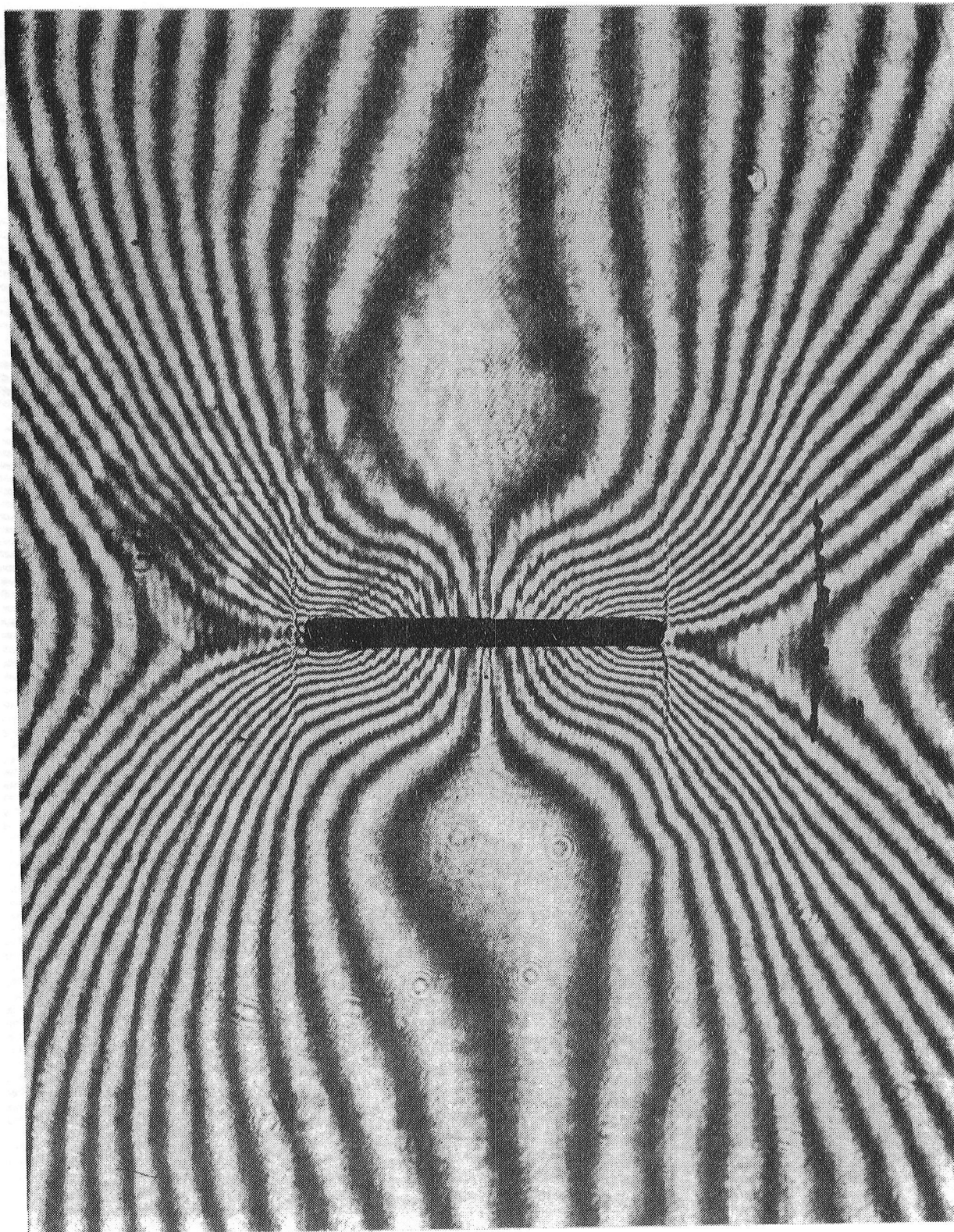


Fig. 3 (h). N_x pattern for $P/P_f = 60\%$.

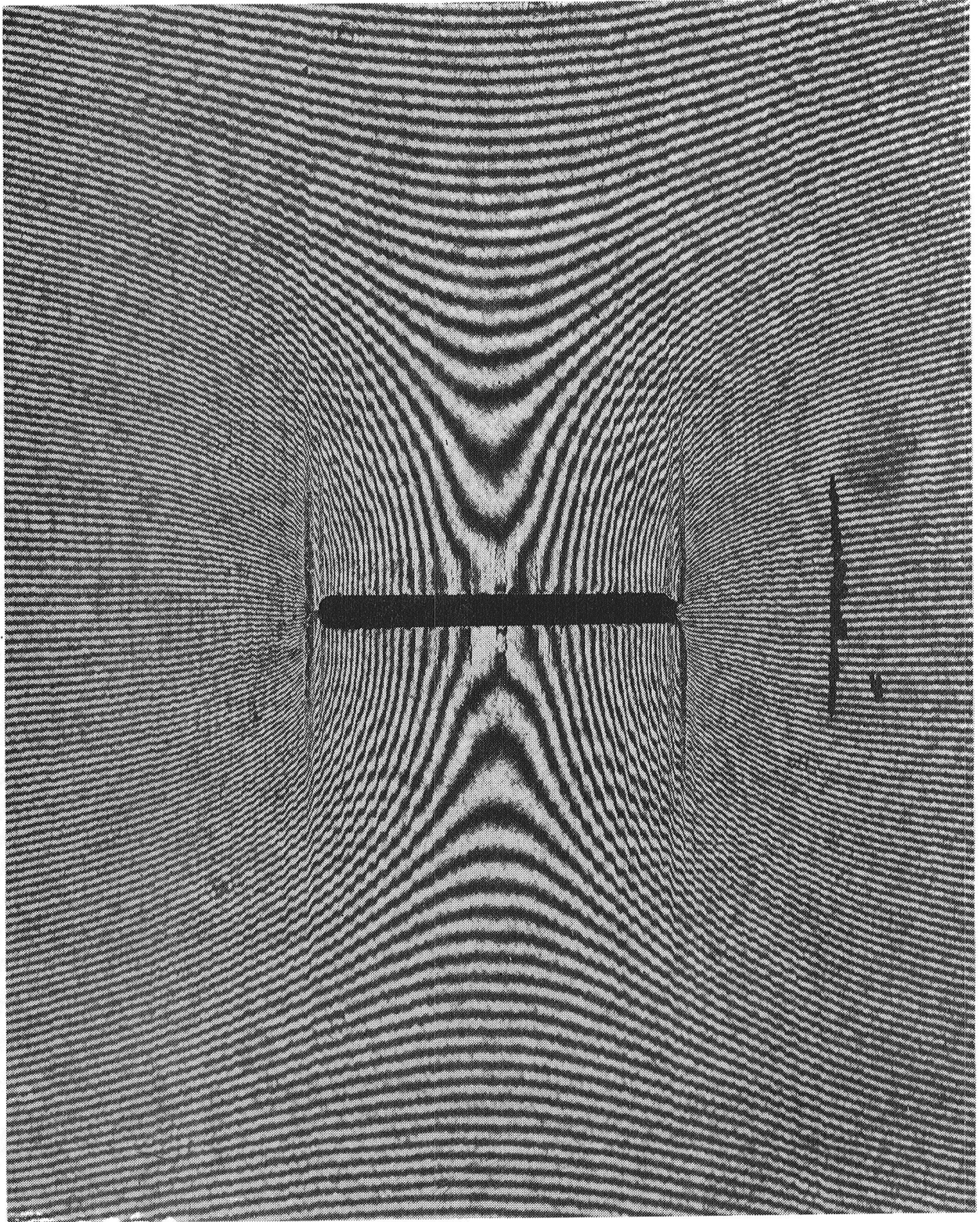


Fig. 3 (i). N_y pattern for $P/P_f = 80\%$.

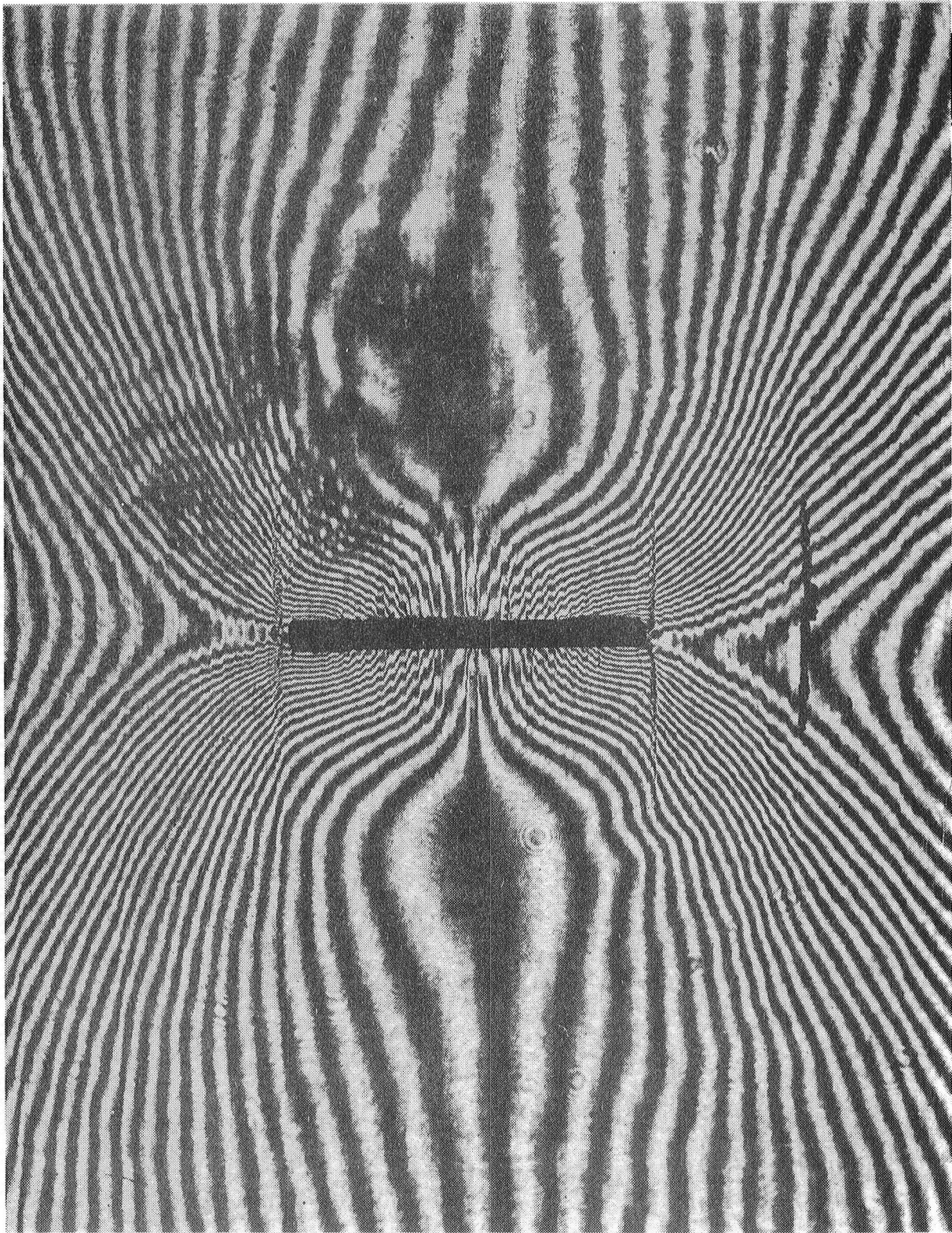


Fig. 3 (j). N_y pattern for $P/P_f = 80\%$.

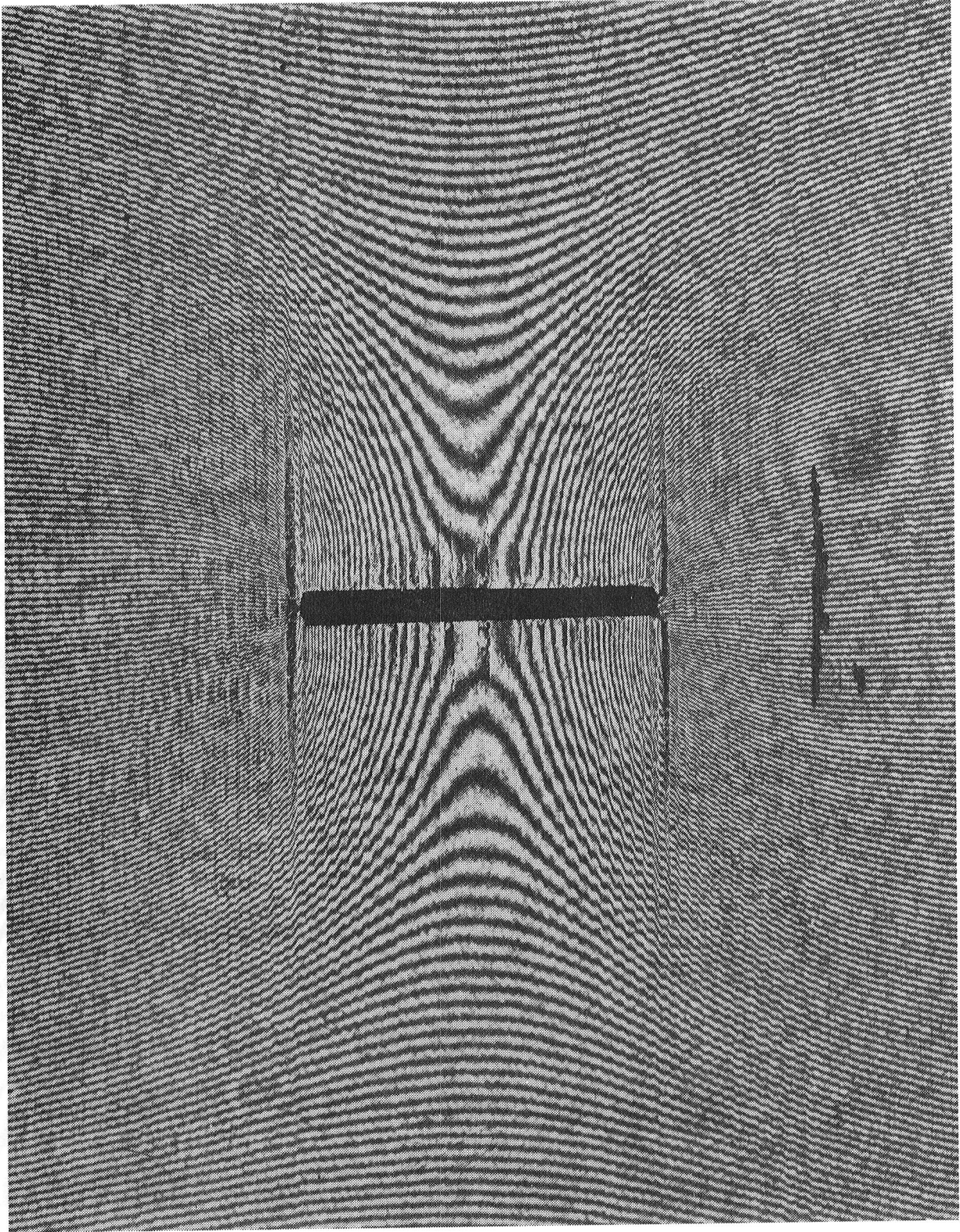


Fig. 3 (k). N_y pattern for $P/P_f = 95\%$.

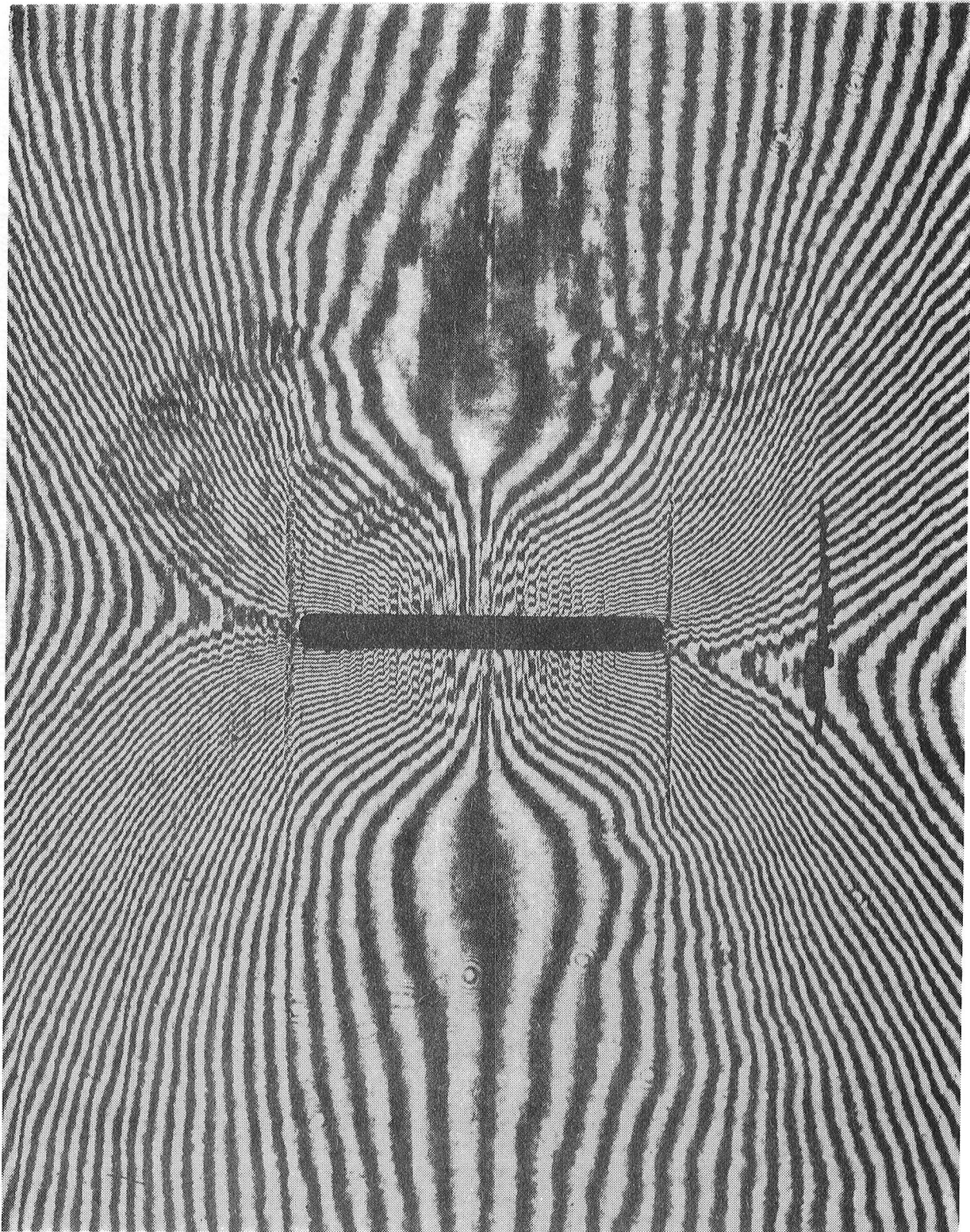


Fig. 3 (1). N_x pattern for $P/P_f = 95\%$.

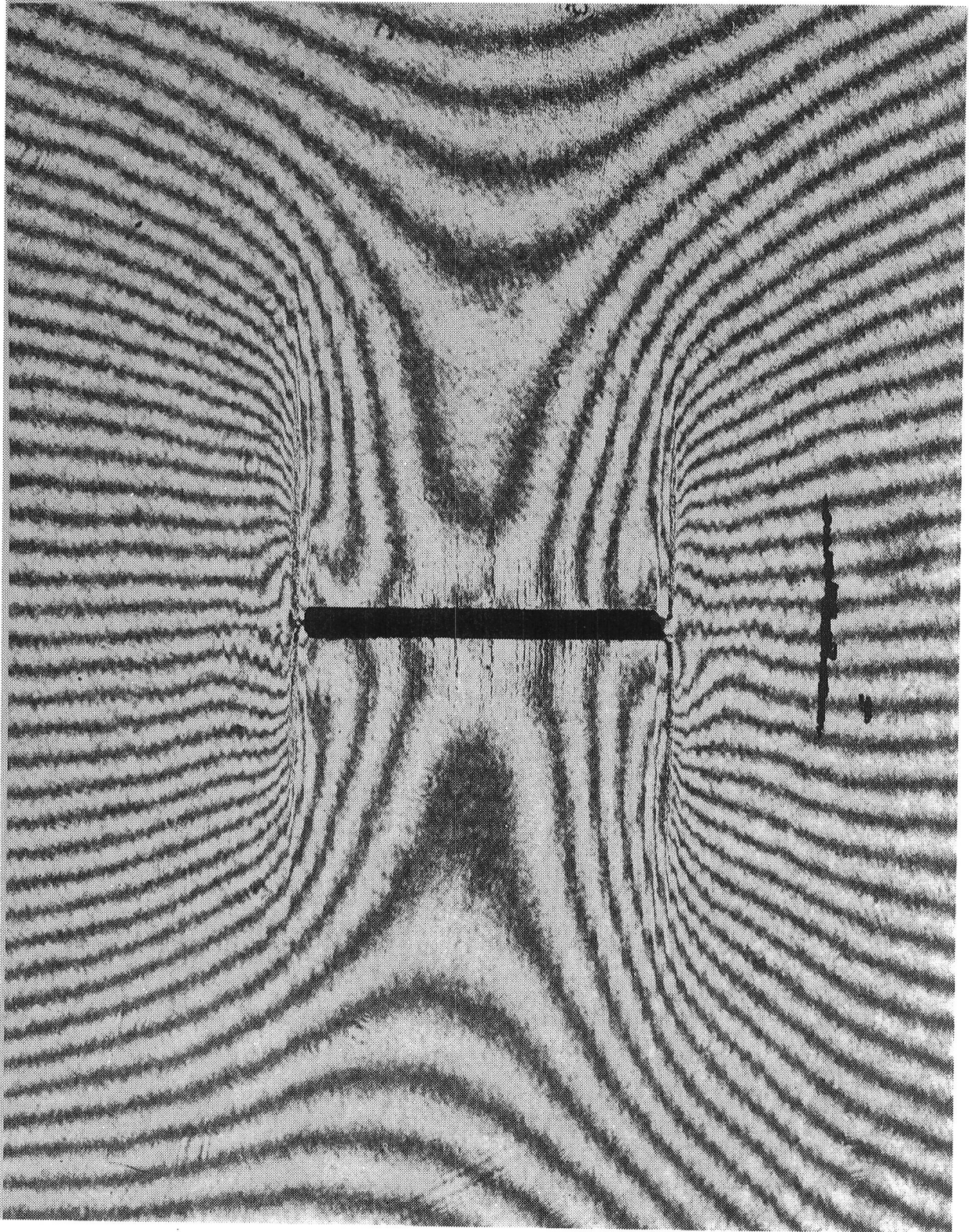


Fig. 4 (a). N_y pattern depicting the residual u_y displacement field after specimen was unloaded to $P/P_f = 1.3\%$.

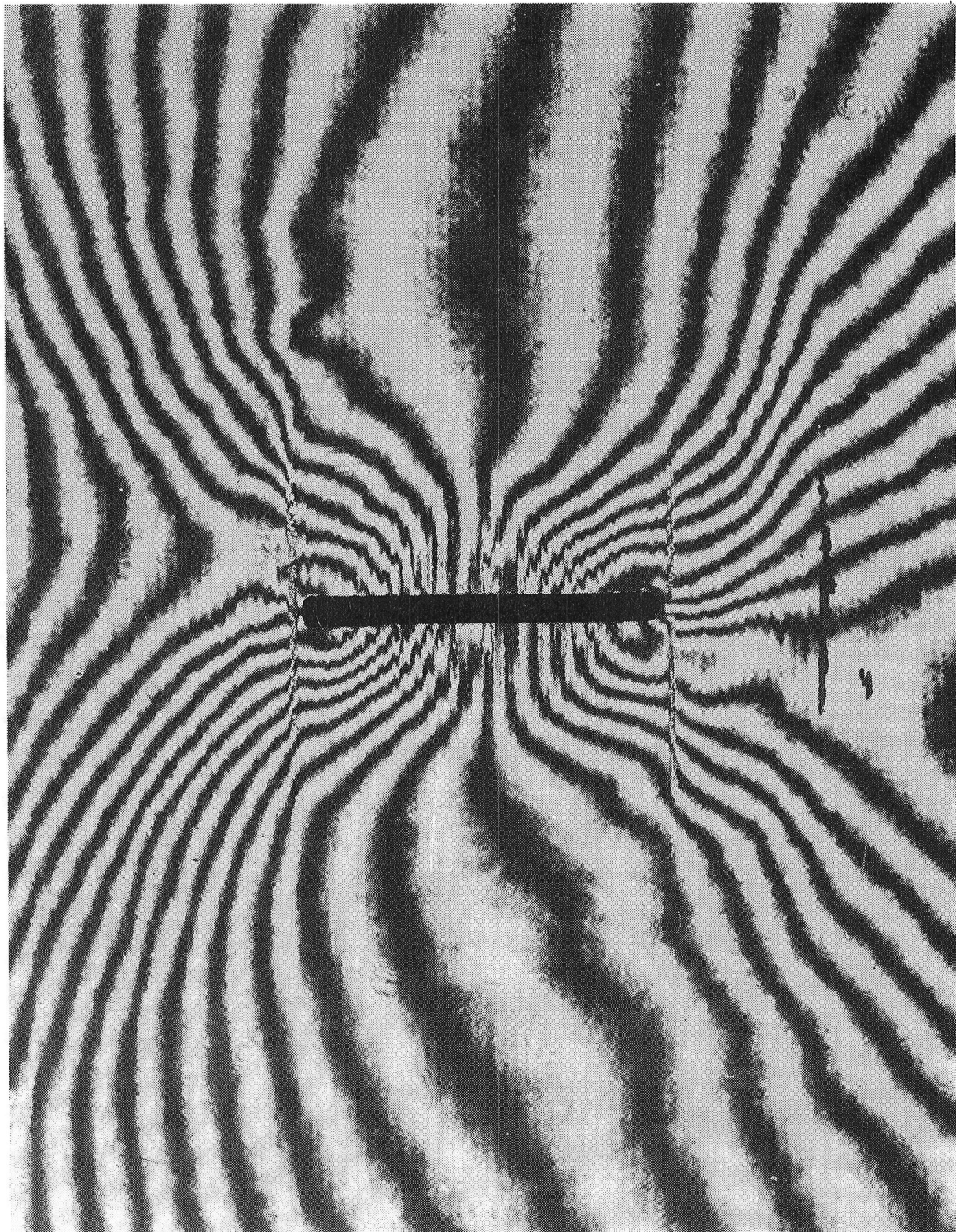


Fig. 4 (b). Residual N_x pattern for $P/P_f = 1.3\%$.

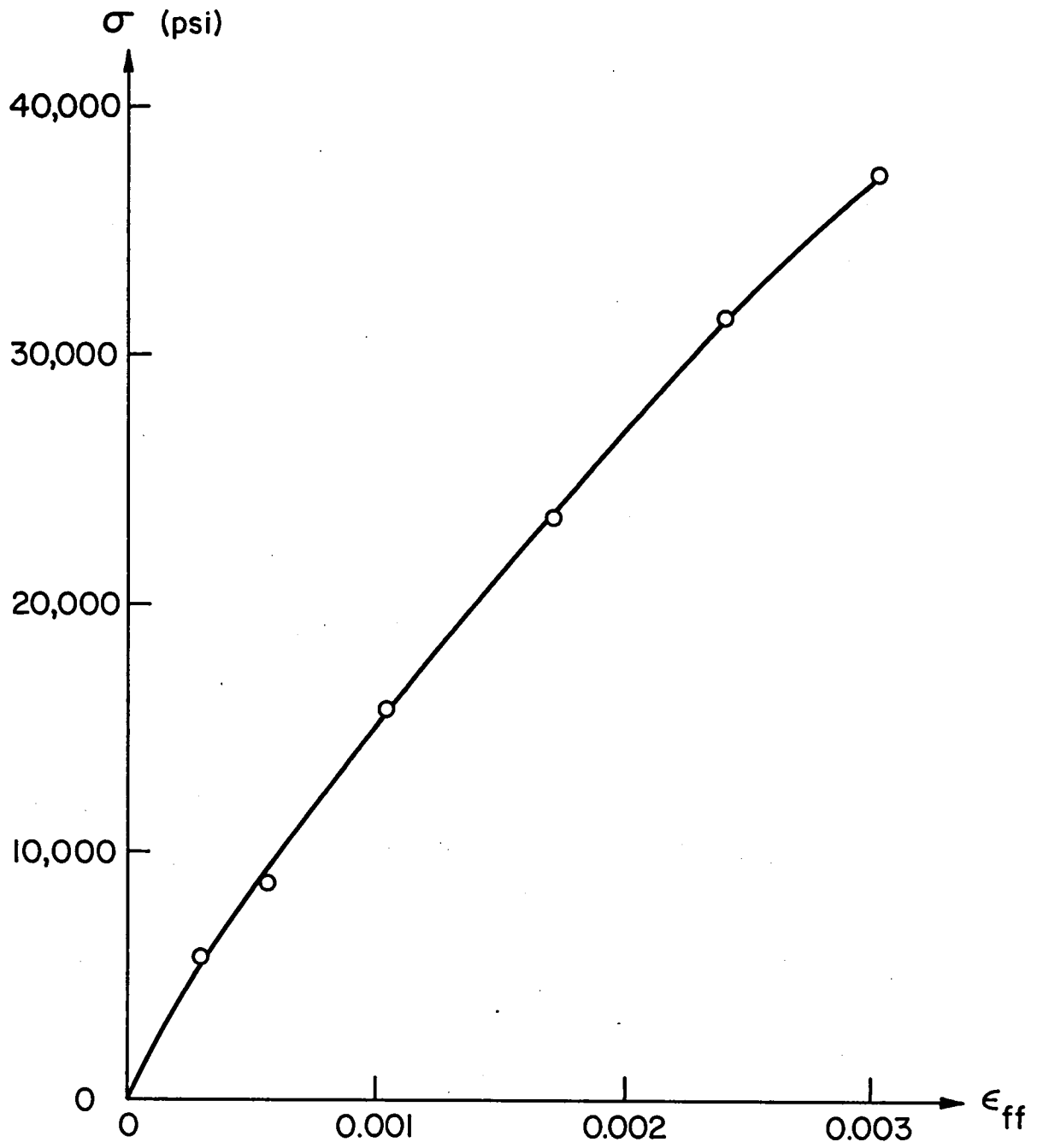


Fig. 5 Longitudinal stress vs. strain for the specimen remote from the slot. Strains were measured by the strain gage. Subscript ff denotes far field.

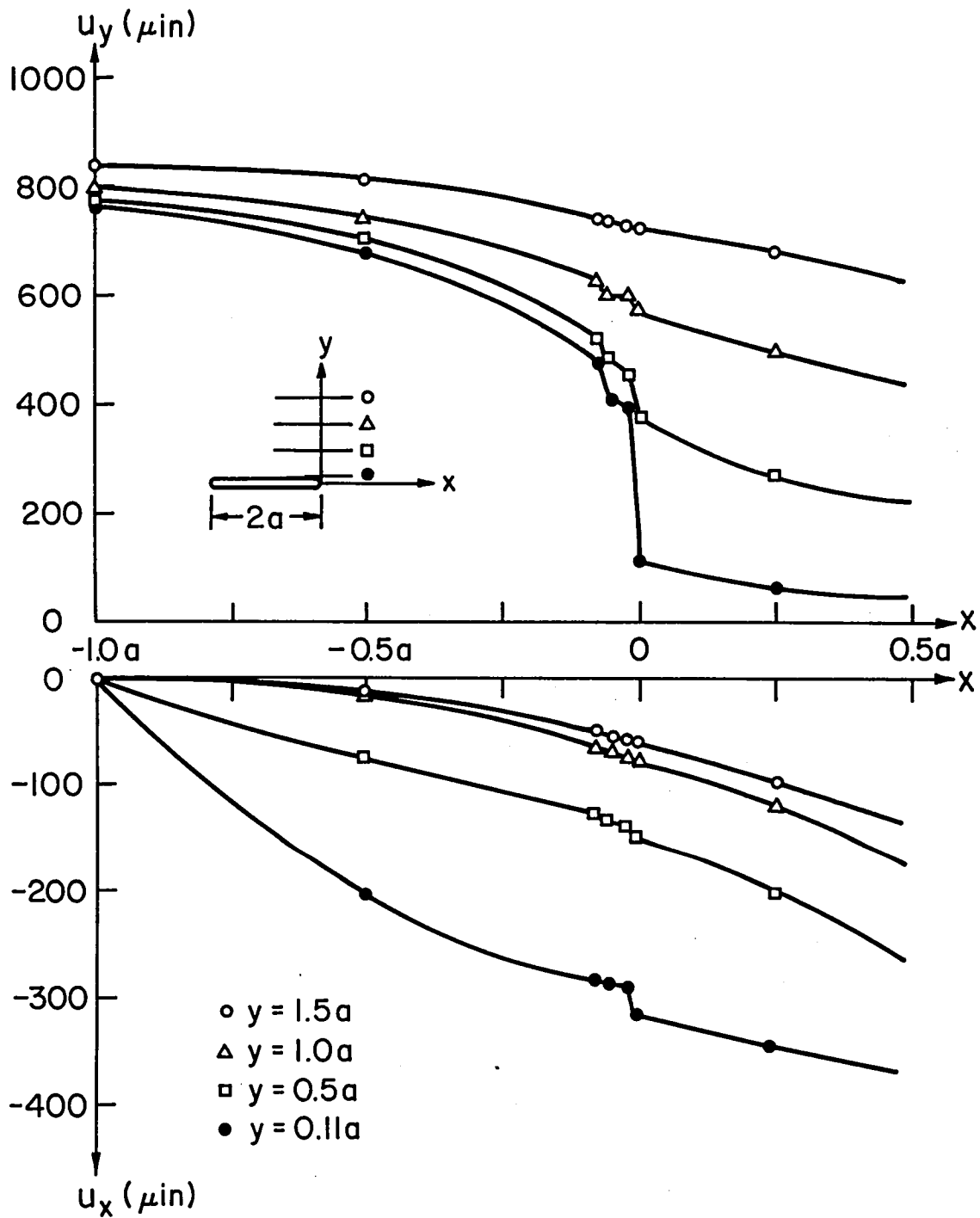


Fig. 6 Deformation near the slot for $P/P_f = 80\%$. Displacements u_y and u_x are plotted vs. position for 4 horizontal lines.

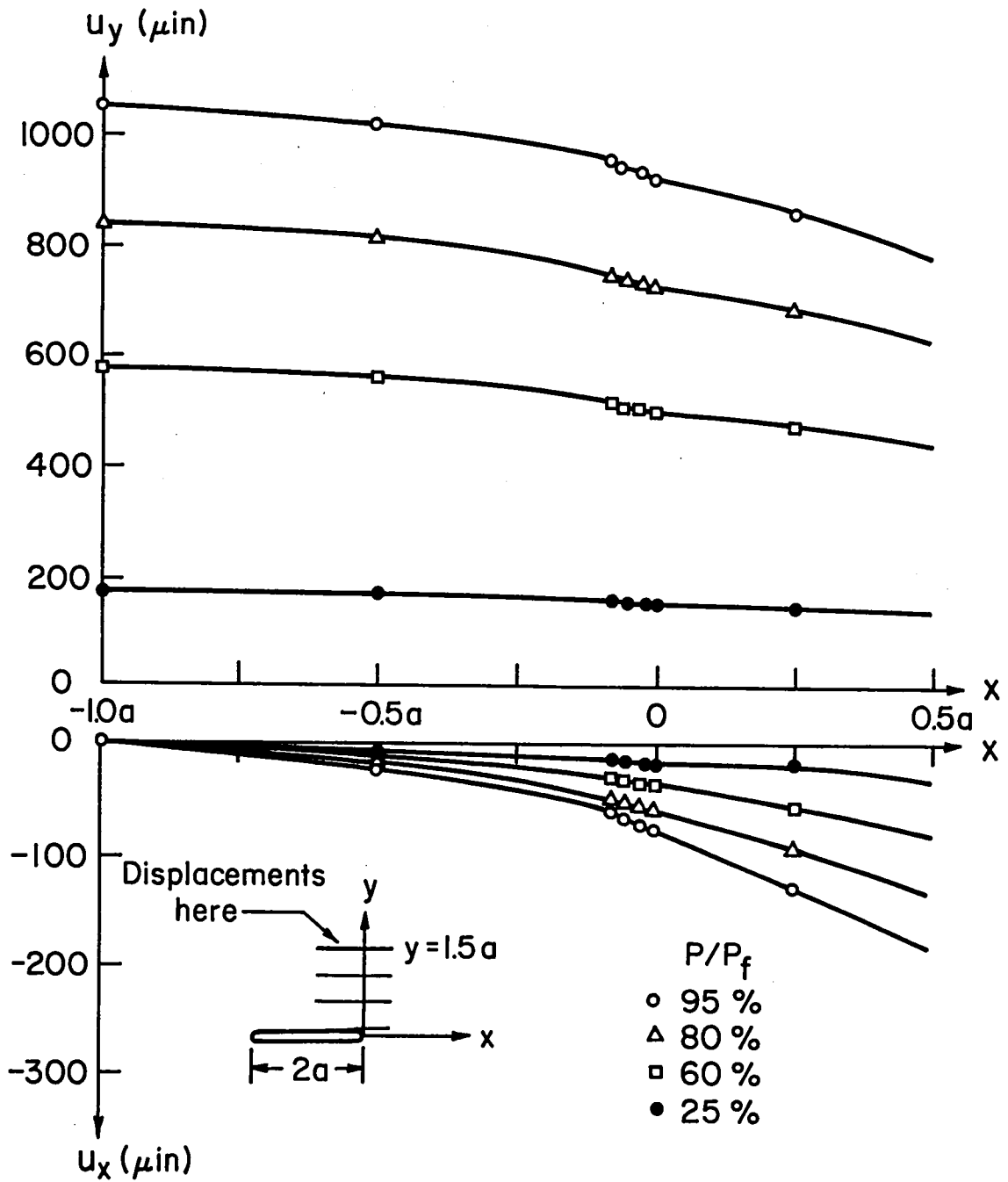


Fig. 7 (a). Displacements u_y and u_x along line $y = 1.5a$ for 4 load levels.

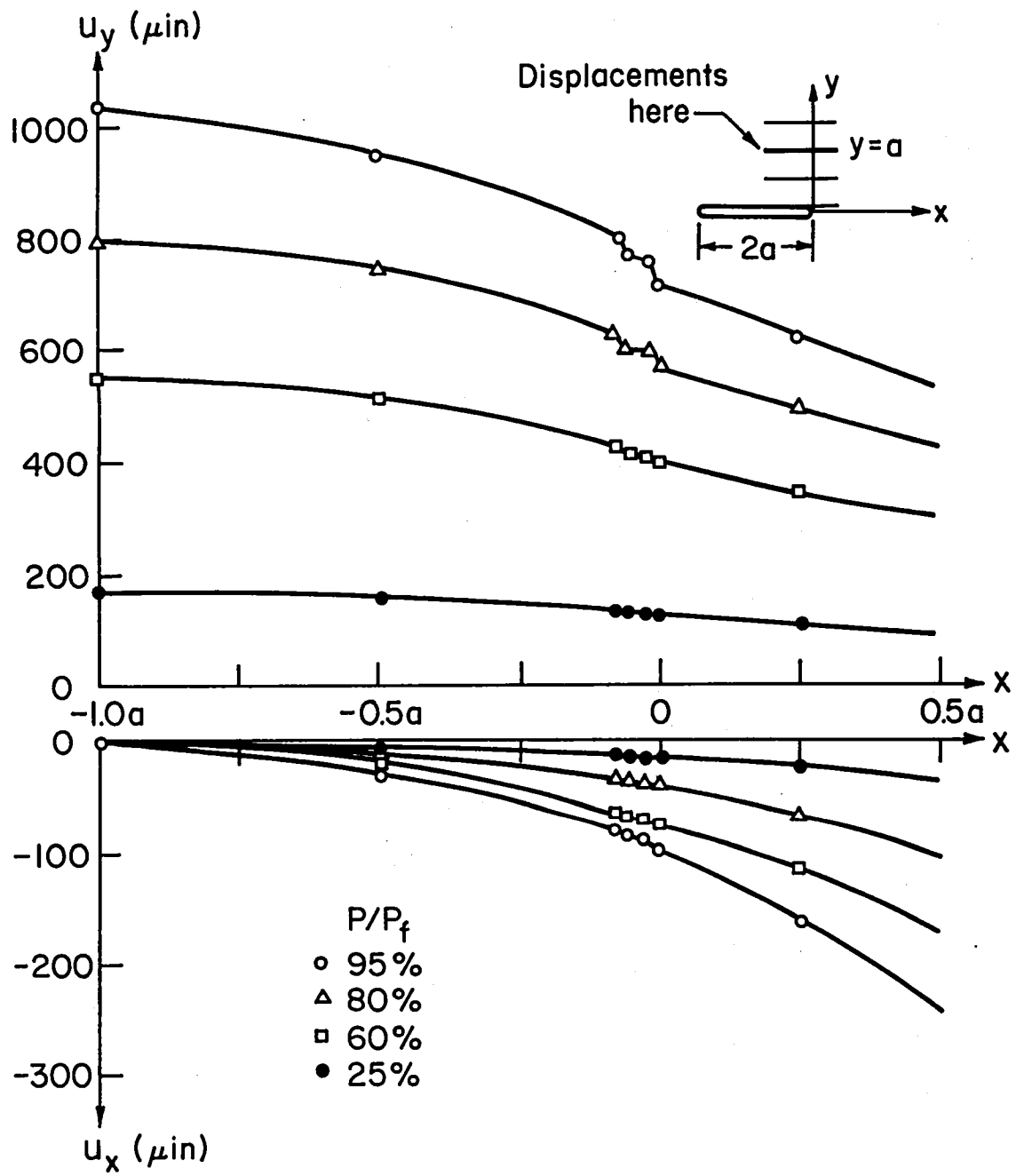


Fig. 7 (b). Displacements u_y and u_x along line $y = a$ for 4 load levels.

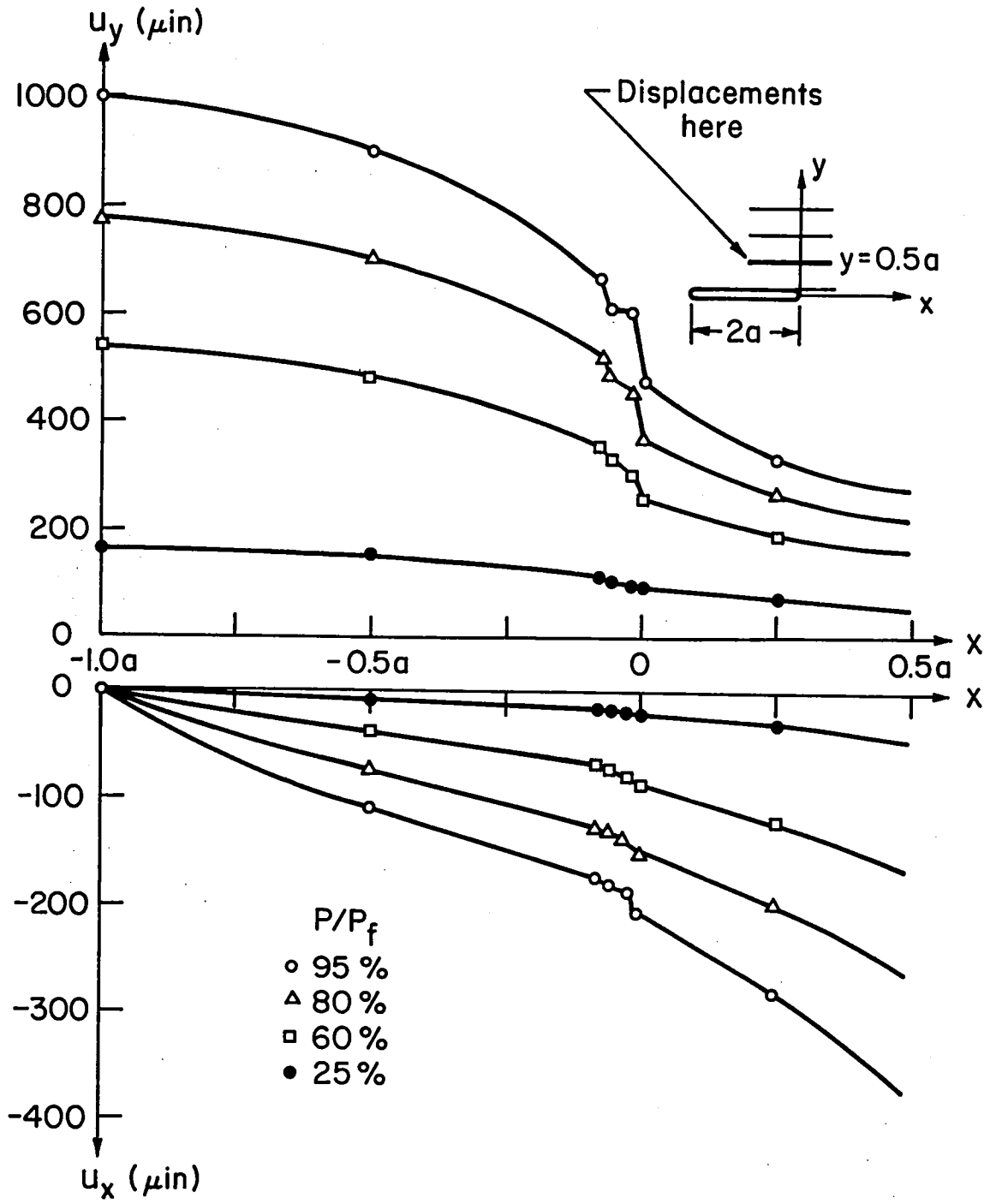


Fig. 7 (c). Displacements u_y and u_x along line $y = 0.5a$ for 4 load levels.

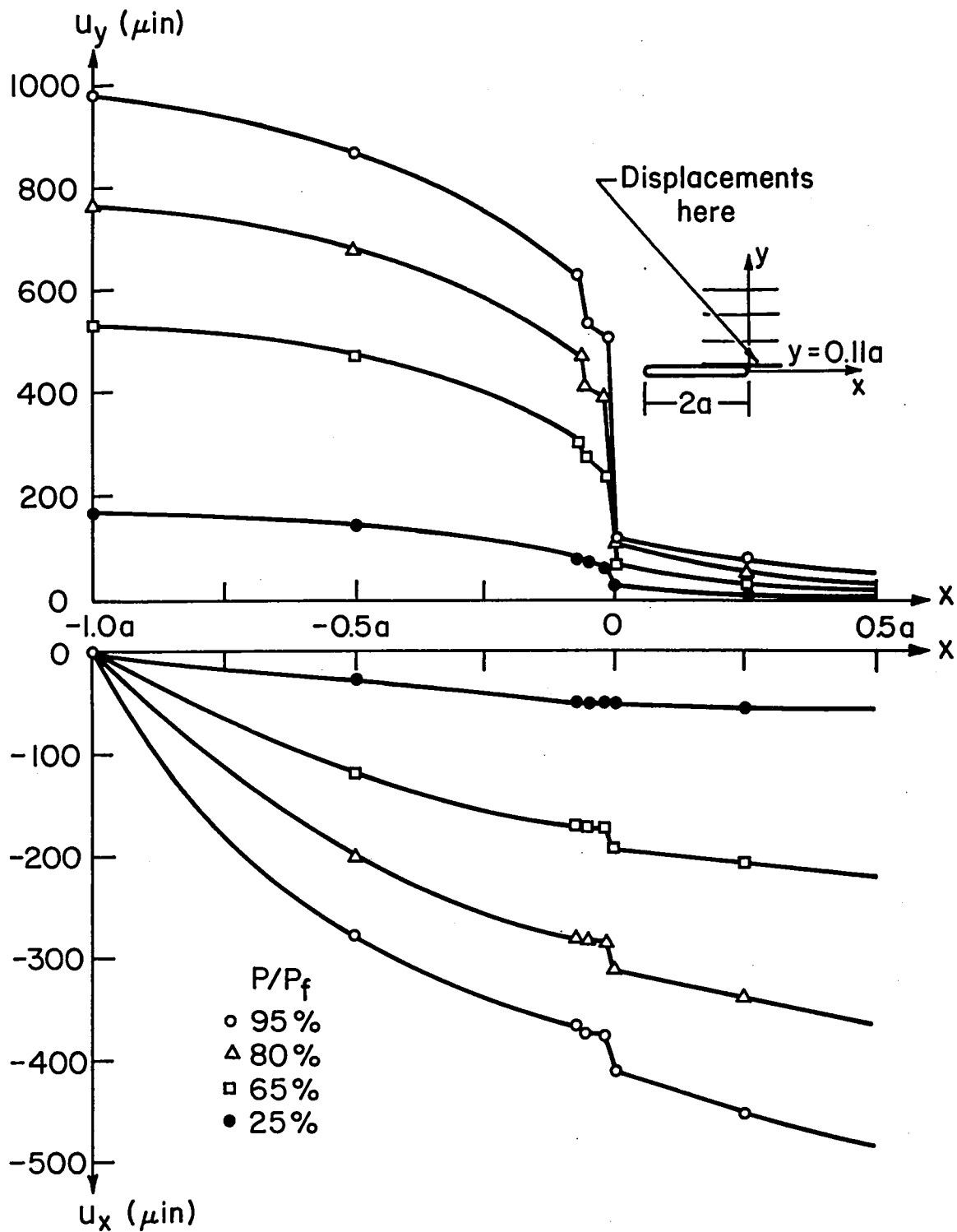


Fig. 7 (d). Displacements u_y and u_x along line $y = 0.11a$ (tangent to edge of slot) for 4 load levels.

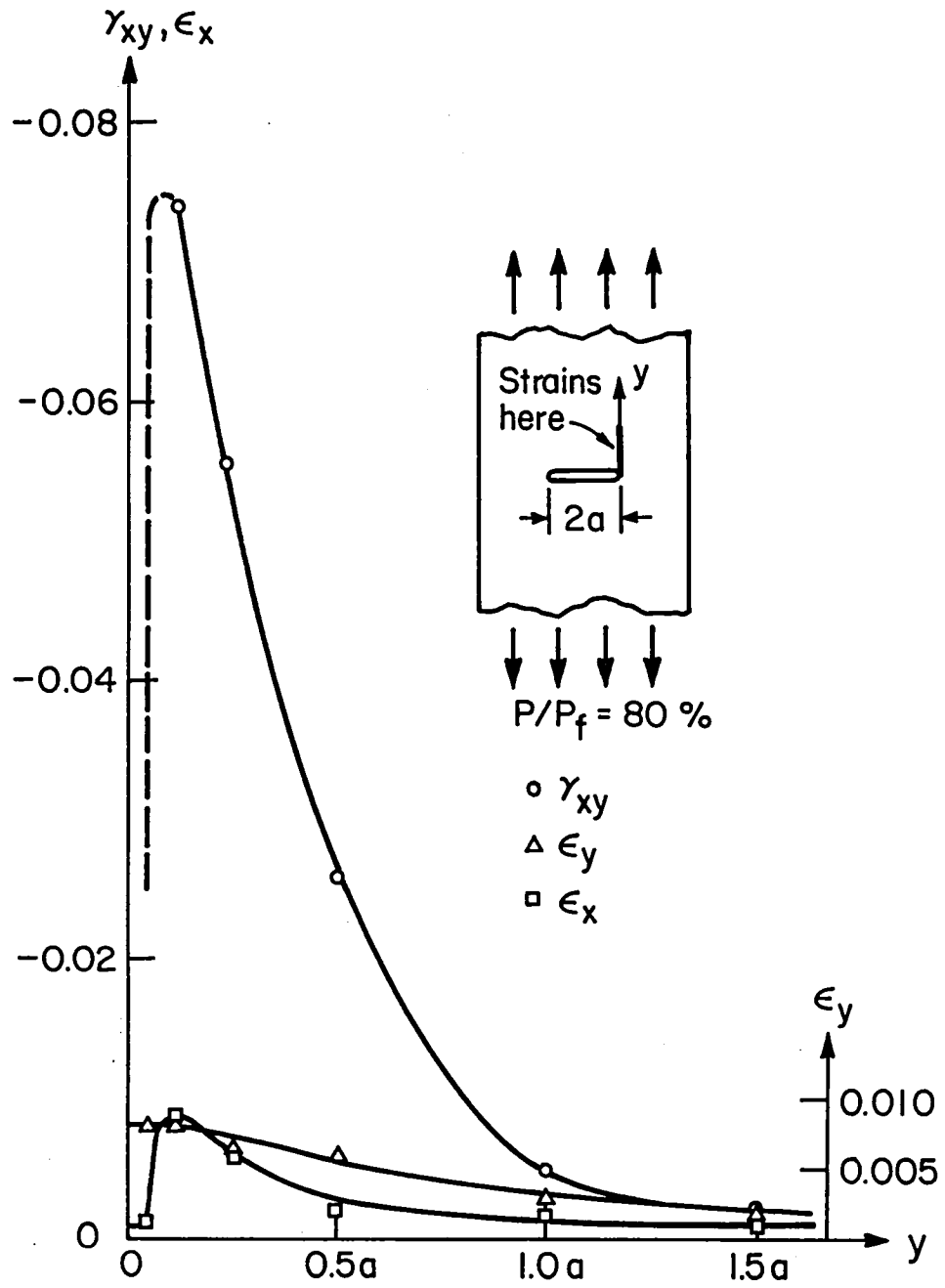


Fig. 8 (a). Normal and shear strains along the y axis.

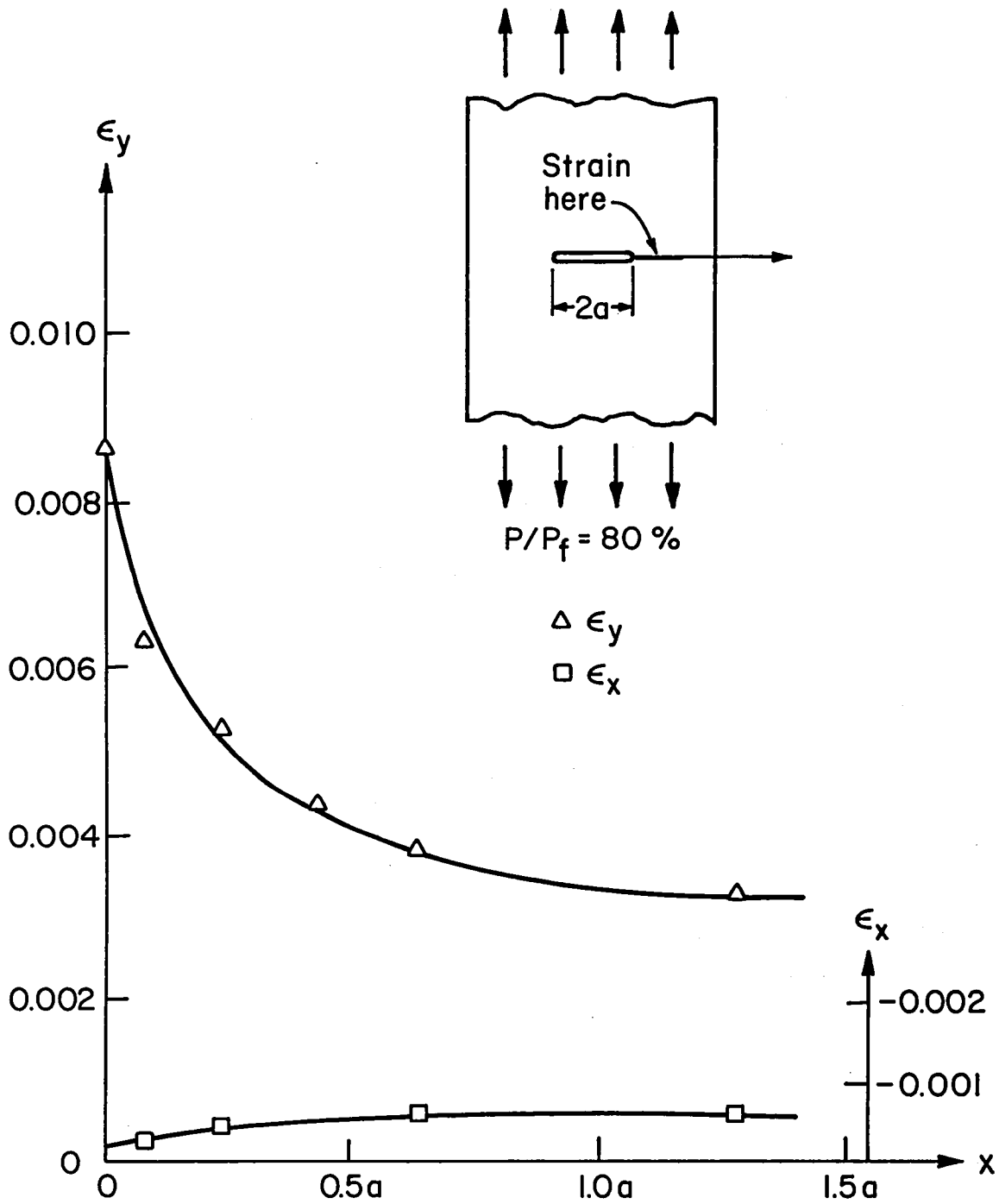


Fig. 8 (b). Normal strains along the x axis.

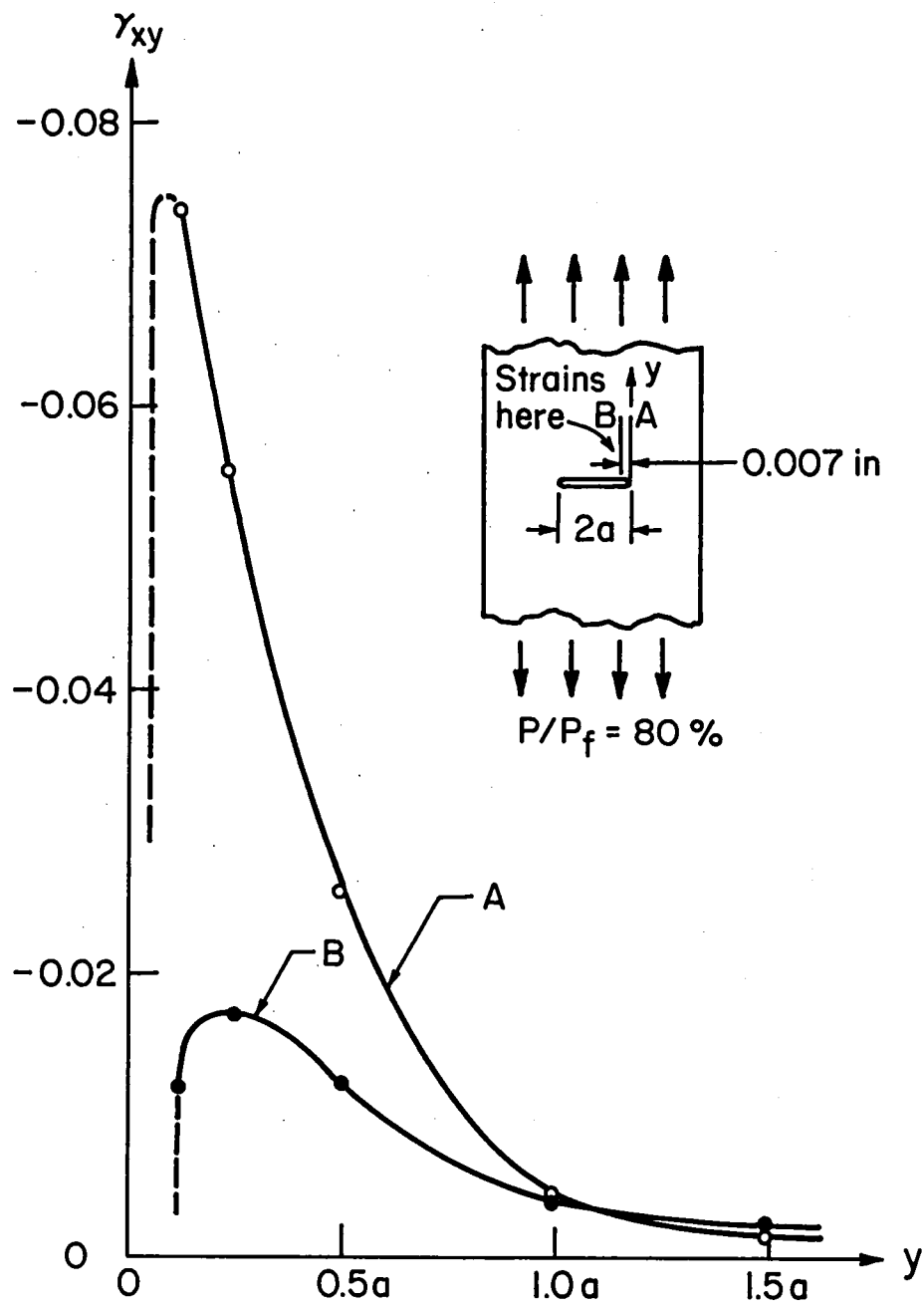


Fig. 9 Comparison of shear strains along lines A and B.

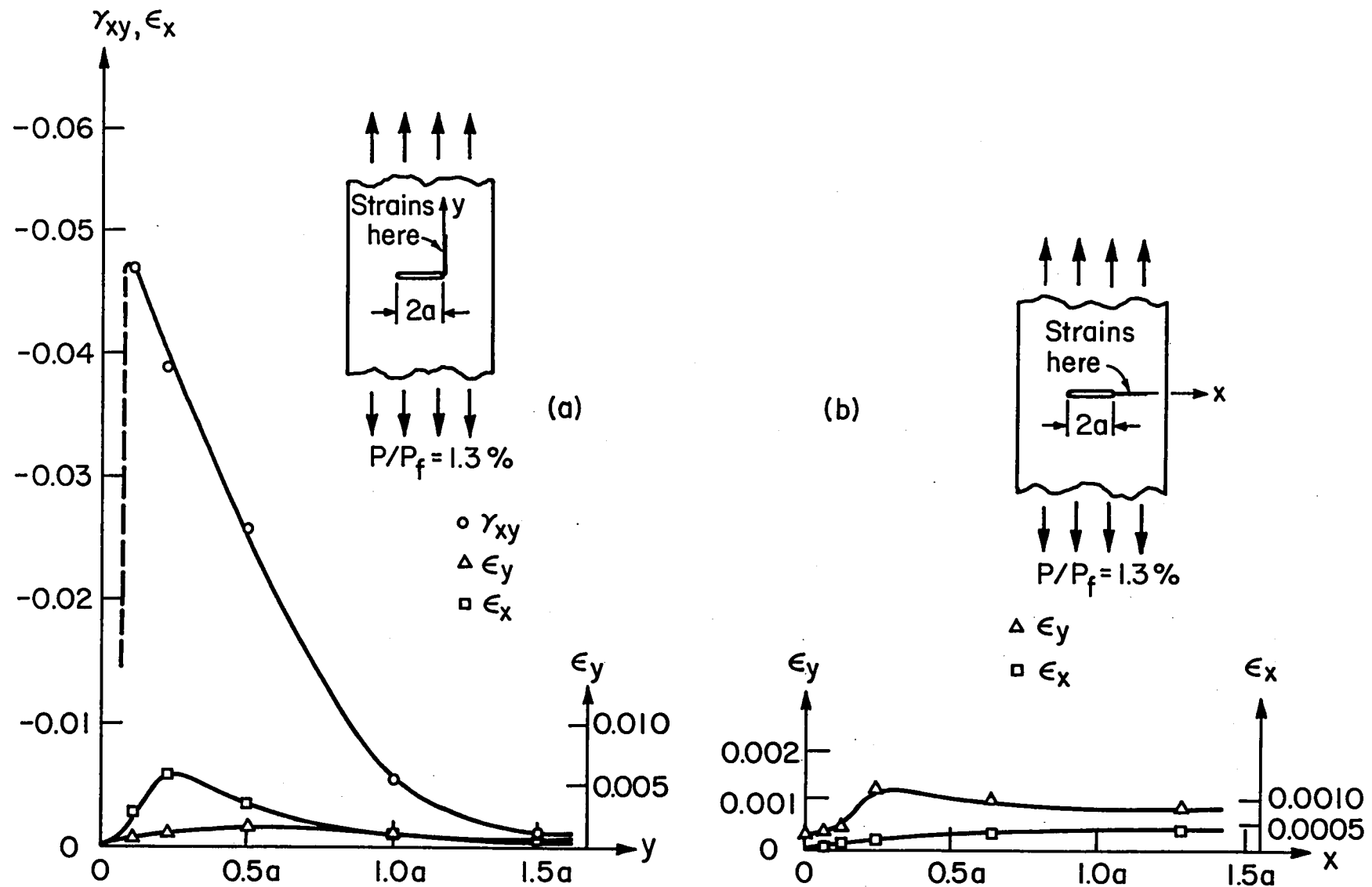


Fig. 10 (a). Residual strains along the y axis.
 (b). Residual strains along the x axis.

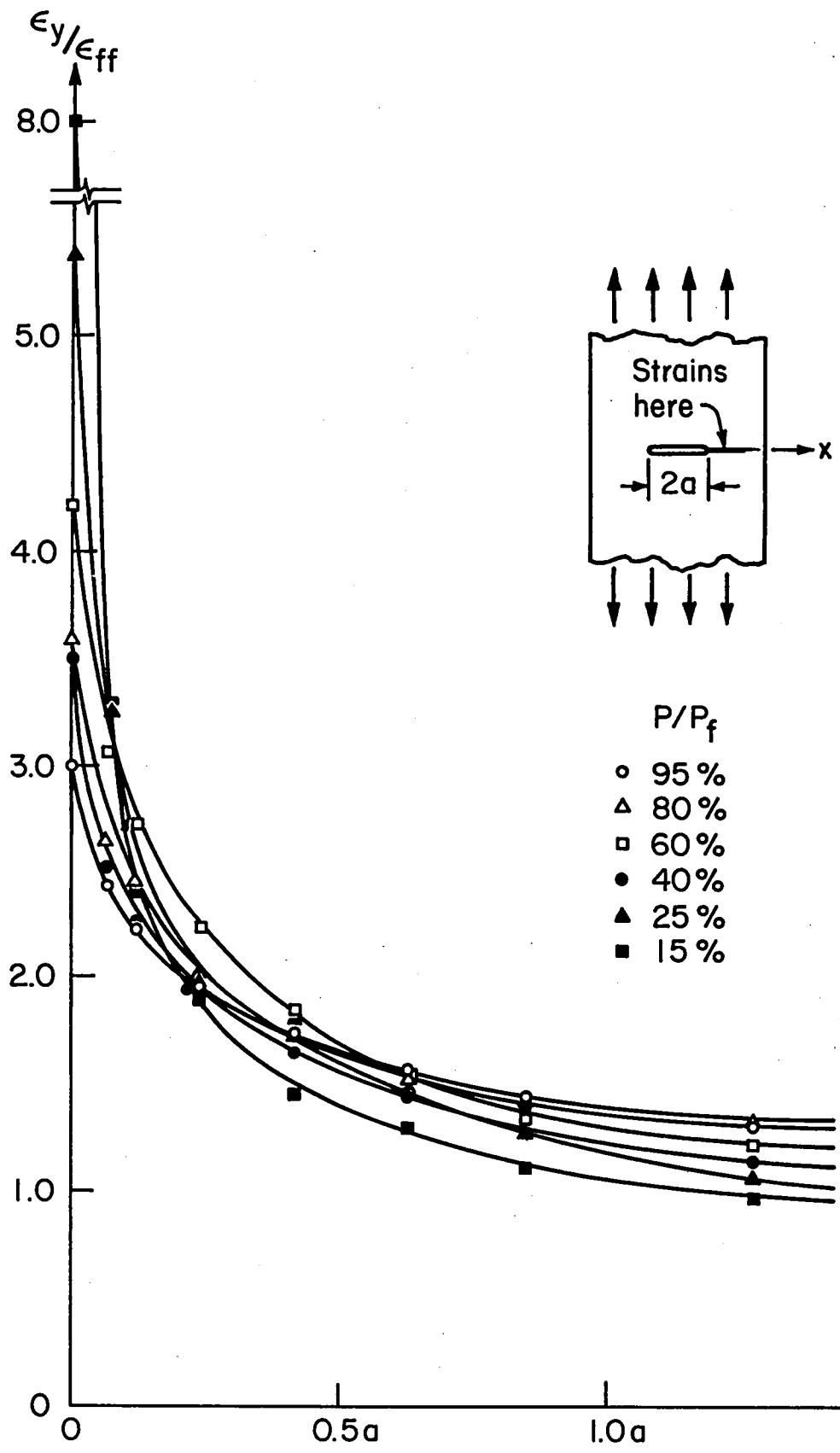


Fig. 11 (a). Strains ϵ_y along the x axis, normalized with respect to the far-field strain, ϵ_{ff} .

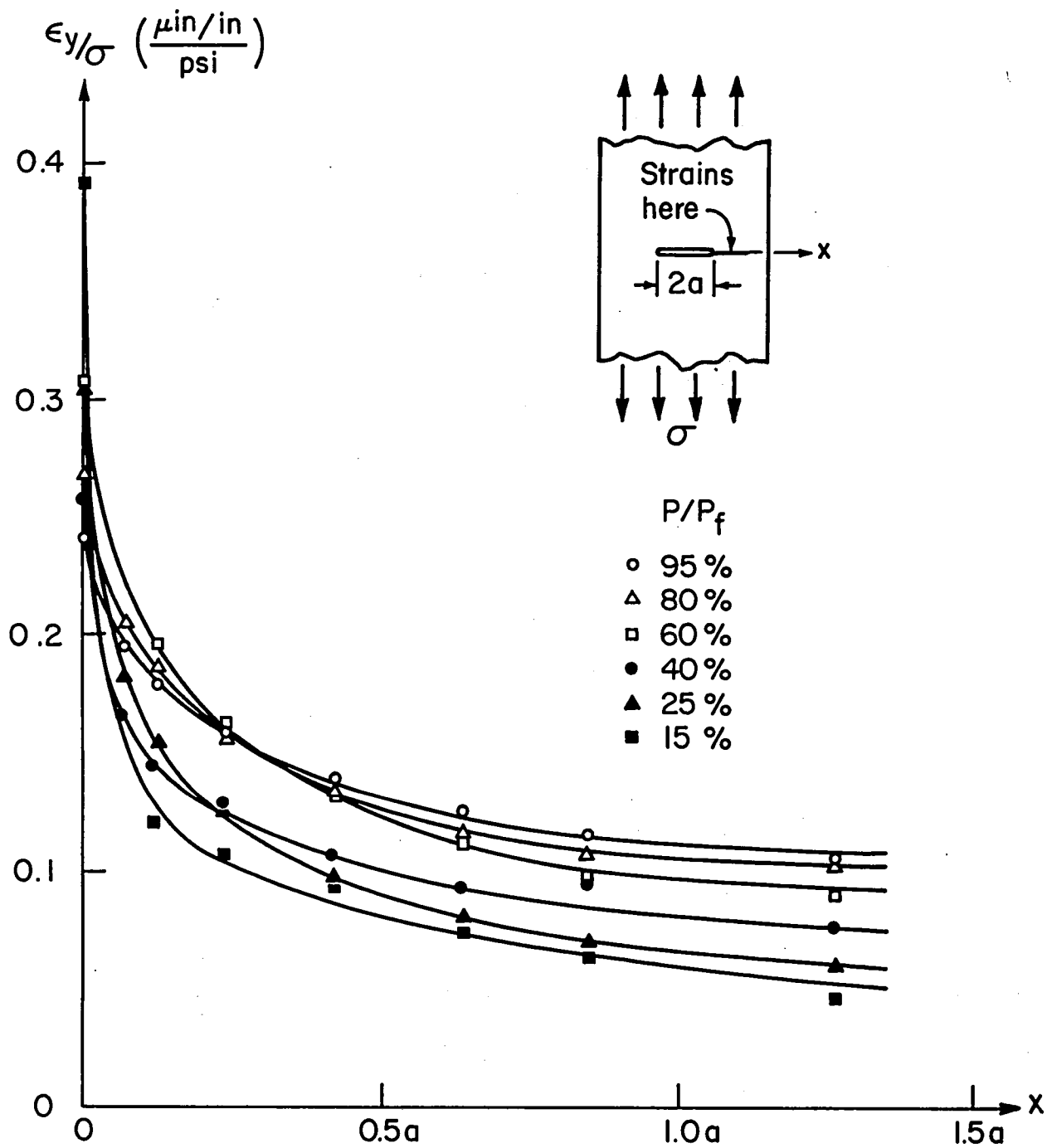


Fig. 11 (b). Strains ϵ_y along the x axis, normalized with respect to the far-field stress, σ .

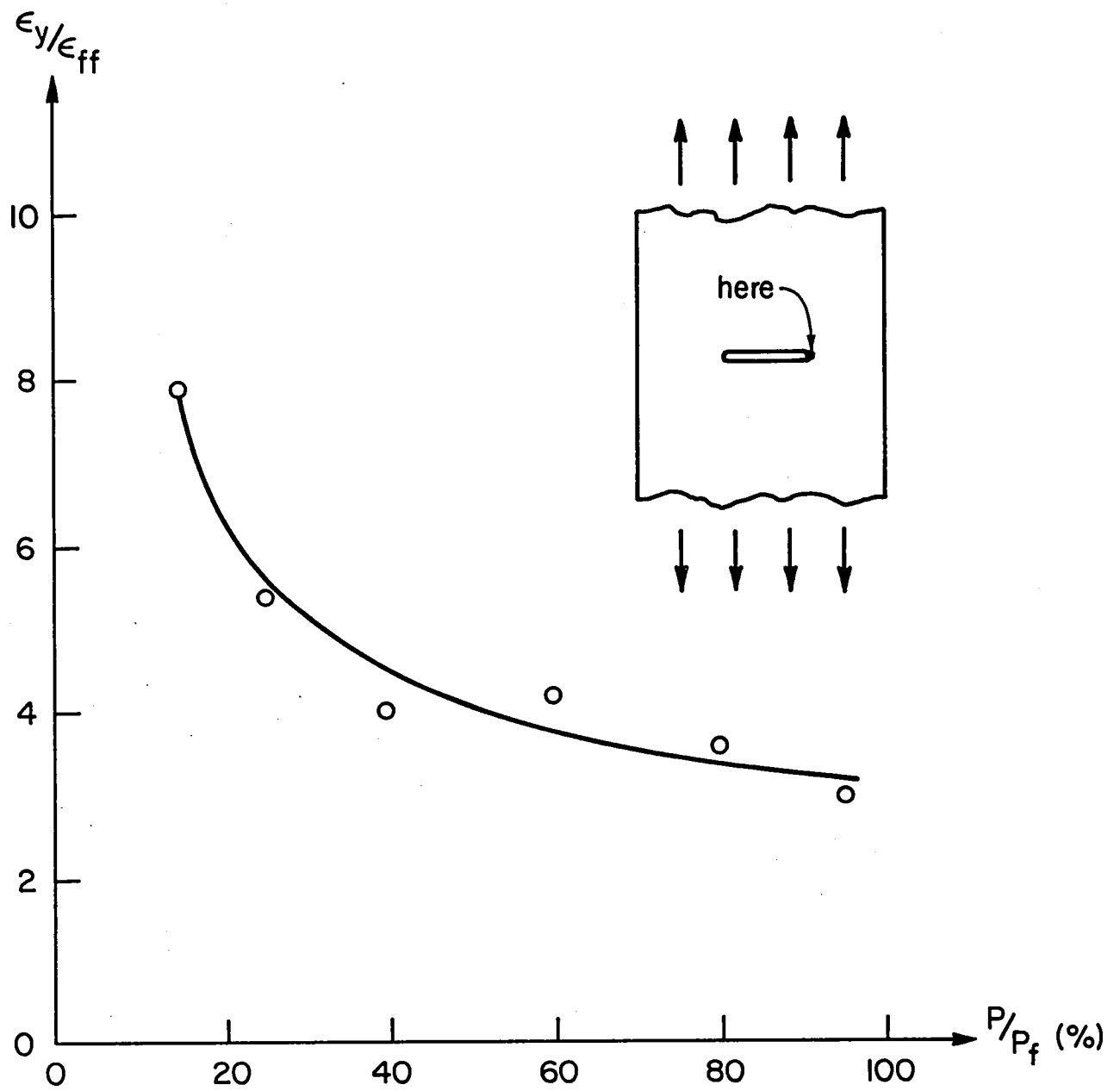


Fig. 12 Strain concentrations ϵ_y/ϵ_{ff} at $x = y = 0$, vs. load level.

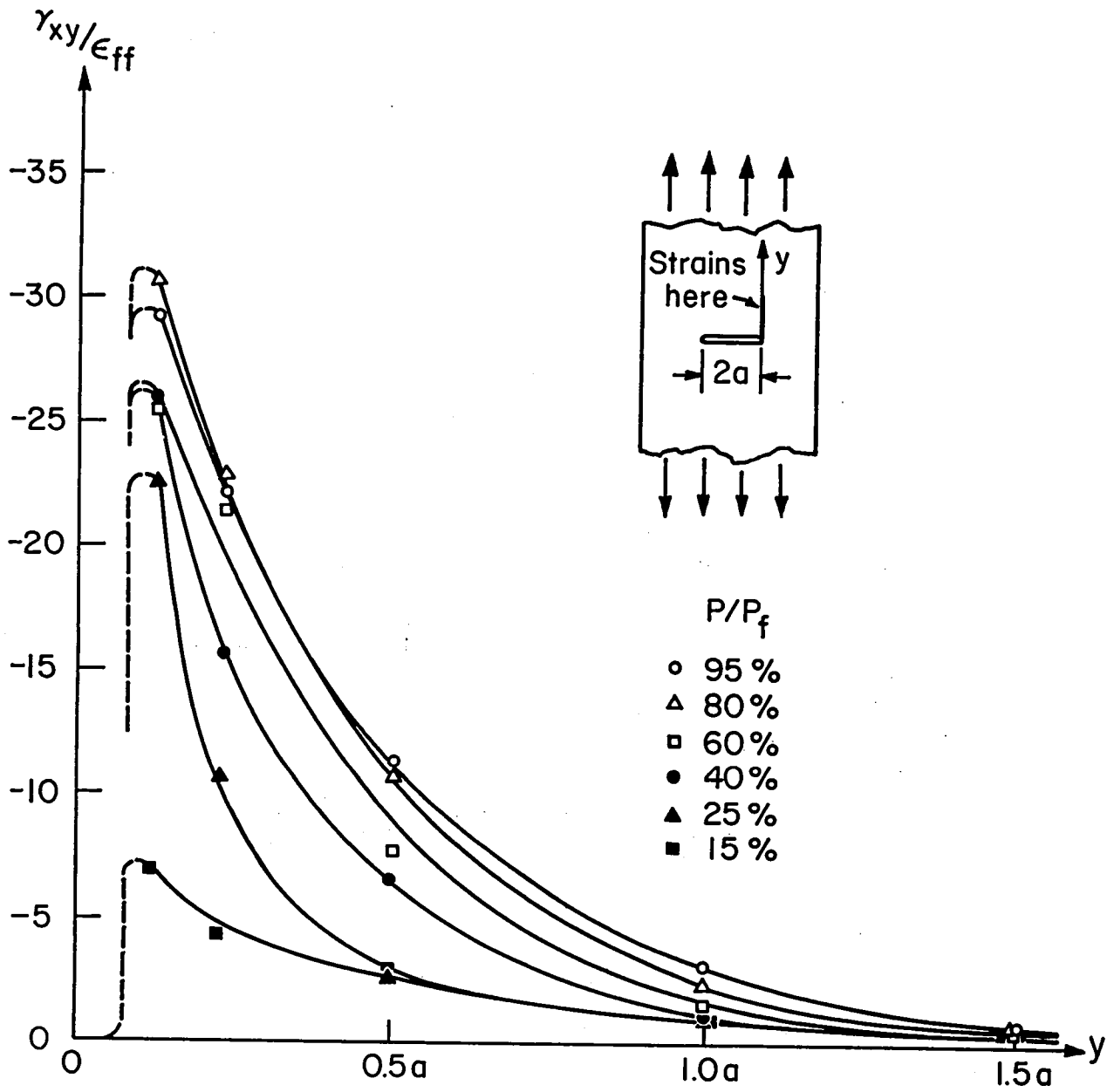


Fig. 13 (a). Shear strains γ_{xy} along the y axis, normalized with respect to the far-field strain, ϵ_{ff} .

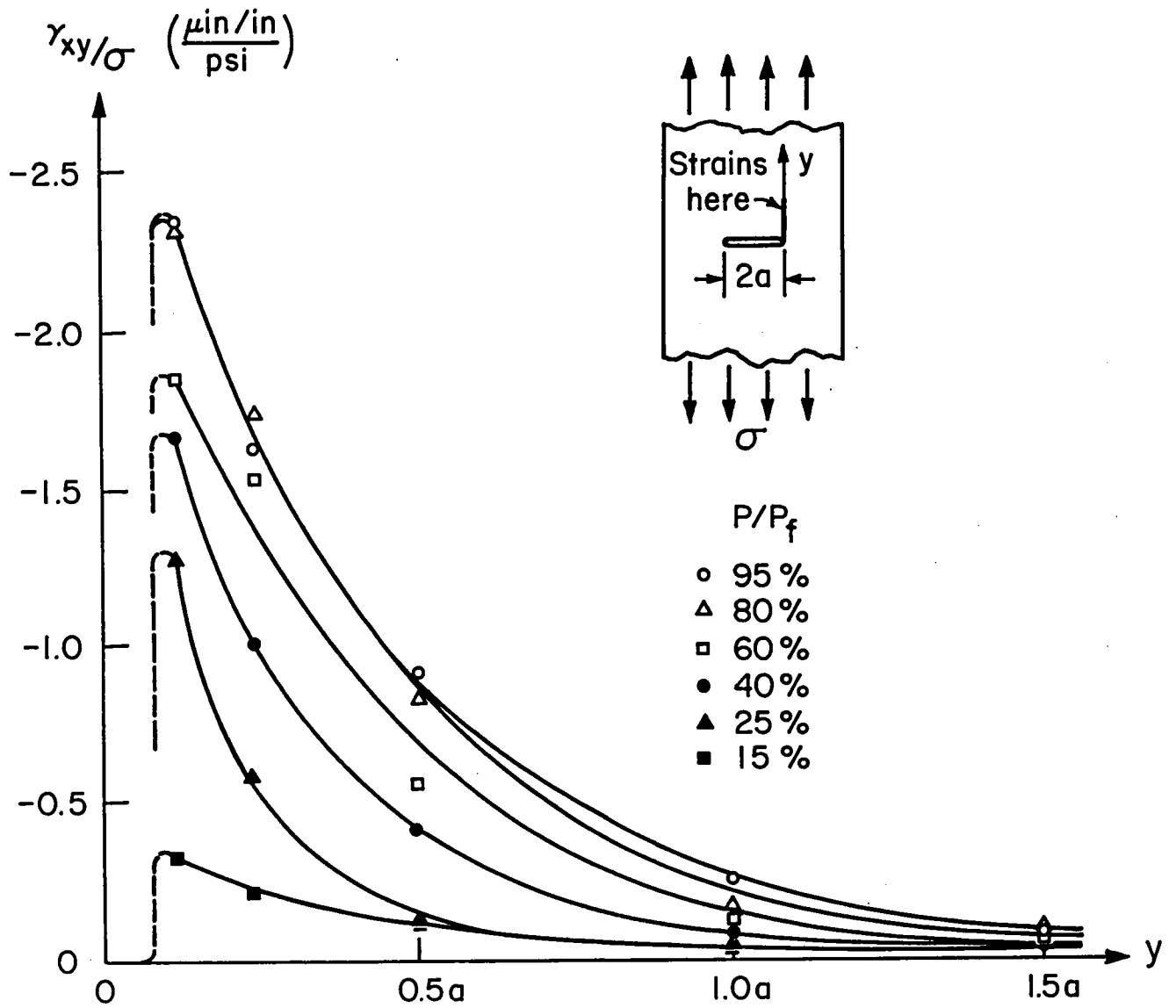


Fig. 13 (b). Shear strains γ_{xy} along the y axis, normalized with respect to the far-field stress, σ .

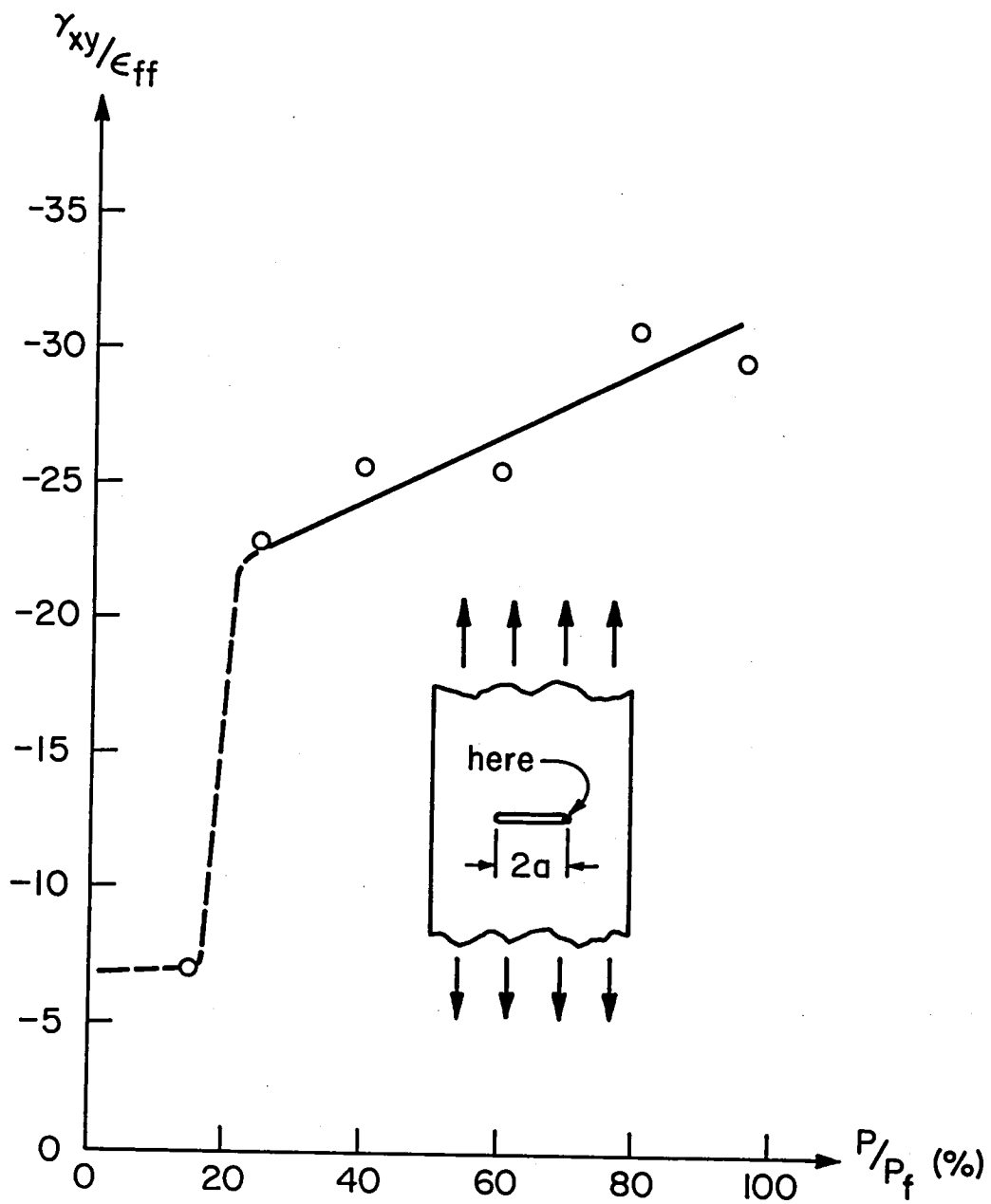


Fig. 14 Shear strain concentrations $\gamma_{xy}/\epsilon_{ff}$ at point where shear strain γ_{xy} is maximum, vs. load level.



Standard Bibliographic Page

1. Report No. NASA CR-178013		2. Government Accession No.		3. Recipient's Catalog No.	
4. Title and Subtitle ELASTIC-PLASTIC DEFORMATION OF A METAL-MATRIX COMPOSITE COUPON WITH A CENTRAL SLOT				5. Report Date November 1985	
				6. Performing Organization Code	
7. Author(s) Daniel Post, Robert Czarnek, Duksung Joh, Jinmyun Jo, and Yifan Guo				8. Performing Organization Report No.	
				10. Work Unit No.	
9. Performing Organization Name and Address Virginia Polytechnic Institute and State University Engineering Science and Mechanics Dept. Blacksburg, VA 24061				11. Contract or Grant No. NAG1-343	
				13. Type of Report and Period Covered Contractor Report	
12. Sponsoring Agency Name and Address National Aeronautics and Space Administration Washington, DC 20546				14. Sponsoring Agency Code 506-43-11-04	
				15. Supplementary Notes Langley Technical Monitor: W. Steven Johnson	
16. Abstract A comprehensive experimental analysis of deformations of the surface of a metal-matrix specimen is reported. The specimen was a 6-ply [0/+ 45] boron-aluminum tensile coupon with a central slot. Moire interferometry was used for high-sensitivity whole-field measurements of in-plane displacements. Normal and shear strains were calculated from displacement gradients. Displacement fields were analyzed at various load levels from 15% to 95% of the failure load. Deformations of the boron fibers could be distinguished from those of the matrix. Highly localized plastic slip zones occurred tangent to the ends of the slot. Shear strains and concurrent transverse compressive strains in the slip zones reached approximately 10% and 1%, respectively. Upon unloading, elastic recovery in surrounding regions caused a reverse plastic shear strain in the slip zone of about 4%. Longitudinal normal strains on the unslotted ligament peaked at the slot boundary at about 1% strain. The strain concentration factor at the end of the slot decreased with load level and the advance of plasticity.					
17. Key Words (Suggested by Authors(s)) Composites Plastic slip Metal-matrix Moire interferometry Elastic-plastic Experimental analysis Deformation fields Strain distributions			18. Distribution Statement Unclassified - Unlimited Subject Category 27		
19. Security Classif.(of this report) Unclassified		20. Security Classif.(of this page) Unclassified		21. No. of Pages 48	22. Price A03



